Screening the human druggable genome identifies ABHD17B as an anti-fibrotic target in hepatic stellate cells

Wenyang Li[1,2†], Robert P. Sparks[1,2†], Cheng Sun[1,2†], Yang Yang[2,3], Lorena Pantano[4], Rory Kirchner[4], Jennifer Y. Chen[1,2], Sean P. Moran[1,2], Victor Barrera[4], David Wrobel[5], Shannan J. Ho Sui[4], Gary Aspnes[6], Michael Schuler[6], Jennifer Smith[5], Benjamin D. Medoff[2,3], Carine M. Boustany-Kari[7], Jörg F. Rippmann[6], Daniela M. Santos[7], Julia F. Doerner[6], Alan C. Mullen[1,2,8,9*]

1. Division of Gastroenterology, Massachusetts General Hospital, Boston, MA, USA
2. Harvard Medical School, Boston, MA, USA
3. Division of Pulmonary and Critical Care Medicine, Massachusetts General Hospital, Boston, MA, USA
4. Harvard Chan Bioinformatics Core, Harvard T.H. Chan School of Public Health, Boston, MA, USA
5. ICCB-Longwood Screening Facility, Harvard Medical School, Boston, MA 02115 USA
6. Boehringer Ingelheim Pharma GmbH & Co. KG, Biberach a.d. Riss, Germany
7. Boehringer-Ingelheim Pharmaceuticals Inc., Ridgefield, CT, USA
8. Harvard Stem Cell Institute, Cambridge, MA, USA
9. Broad Institute, Cambridge, MA, USA

[†] These authors contribute equally.

* Corresponding author. Thier 306B, 55 Fruit Street, Massachusetts General Hospital, Boston, MA 02114, USA.

Current Address: Lazare Research Building, 364 Plantation Street, Division of Gastroenterology, University of Massachusetts Chan Medical School, Worcester, MA 01605, USA

Email: alan.mullen@umassmed.edu

Current Addresses:

Wenyang Li: College of Chemistry and Molecular Engineering, Peking University, Beijing, 100871, China

Jennifer Y. Chen: Department of Medicine, University of California, San Francisco, San Francisco, CA 94115, USA; Liver Center, Department of Medicine, University of California, San Francisco, San Francisco, CA 94143, USA

Background & Aims:

Chronic liver injury leads to activation of hepatic stellate cells (HSCs), which transdifferentiate into HSC myofibroblasts and produce the extracellular matrix (ECM) that forms the fibrotic scar. While the progression of fibrosis is understood to be the cause of end stage liver disease, there are currently no approved therapies directed at interfering with the activity of HSC myofibroblasts.

Methods:

We performed a high-throughput small interfering RNA (siRNA) screen in primary human HSC myofibroblasts targeting RNAs from >9,500 genes to identify those that promote the fibrotic phenotype of HSCs. The screen identified ABHD17B (Abhydrolase domain containing 17B, depalmitoylase), which was evaluated through loss-of -function studies in multiple primary human HSC lines. Structural analysis was performed to identify key amino acids in the hydrolase pocket of ABHD17B, and depalmitoylase inhibitors were evaluated. Protein partners were identified by mass spectrometry (MS), and *Abhd17b-/-* mice were challenged with carbon tetrachloride (CCl_4) as a model of chronic liver injury.

Results:

Depletion of *ABHD17B* promotes the inactivation of HSCs, characterized by reduced *COL1A1* and *ACTA2* expression and accumulation of lipid droplets. RNA-seq and MS analysis also indicated a broader impact on ECM production and cytoskeletal organization. Mice deficient in *Abhd17b* are viable, demonstrate normal liver histology, and are protected from fibrosis in the setting of *in vivo* liver injury. While ABHD17B is a depalmitoylase, inhibiting this function alone is not sufficient to affect the fibrotic activity of HSCs.

Conclusions:

ABHD17B promotes fibrosis through pathways independent of depalmitoylation that include regulating expression of *COL1A1* and other ECM genes and interacting with proteins involved in cytoskeletal organization, contractility, and adhesion. Targeting ABHD17B may have potential as an antifibrotic therapy.

Keywords

Liver fibrosis, hepatic stellate cells, siRNA screen, ABHD17B, depalmitoylase, collagen

Introduction

Cirrhosis, end stage liver disease, and liver failure result from progressive fibrosis in the setting of chronic liver injury. While successful treatment of the underlying cause of injury can reduce the severity of fibrosis, as demonstrated by therapies for hepatitis B and C[1,2], there are limited treatments for other sources of chronic injury, including non-alcoholic fatty liver disease/ metabolic dysfunction-associated steatotic liver disease (NAFLD/MASLD)[3–5]. In other diseases of fibrotic injury, such as primary sclerosing cholangitis (PSC), we currently have no effective treatments other than liver transplantation[6]. The number of patients with chronic liver disease continues to rise with the prevalence of NAFLD/MASLD, which is now estimated at 24% in North America[7] and is the most rapidly increasing indication for liver transplantation[8].

HSC myofibroblasts are the primary cell type responsible for liver fibrosis[9–11]. These reside in the subendothelial space between endothelial cells and hepatocytes[12] and account for ~5-8% of total cells in the liver[13]. In the healthy liver, HSCs are in a quiescent state and store vitamin A as retinol ester in lipid droplets[9,13]. In the setting of chronic injury, HSCs are activated and transdifferentiate into HSC myofibroblasts, characterized by the loss of lipid droplets, increased contractility, and production and secretion of extracellular matrix (ECM) proteins that form the fibrotic scar [12,14].

Resolution of liver fibrosis has been observed when the source of liver injury is removed, such as in patients with successful antiviral therapy against hepatitis B or C[1,2]. In this setting, the HSC population is reduced primarily through apoptosis, while 40-50% of HSC myofibroblast revert to an inactive state, characterized by reduced collagen expression[15,16], suggesting that with the correct signals, HSC myofibroblasts can be directed to an inactive phenotype.

Here, we performed a small interfering RNA (siRNA) screen of the human druggable genome and >2,000 long noncoding (lnc) RNAs to identify genes whose depletion results in HSC

inactivation. We found that depletion of *ABHD17B* (Abhydrolase Domain Containing 17B, depalmitoylase) in primary human HSCs led to a reduction in type I collagen expression and promoted inactivation, and these functions were independent of the depalmitoylase activity of ABHD17B. Furthermore, mice deficient in *Abhd17b* were protected from the development of liver fibrosis. In summary, this study evaluated the effect of siRNAs targeting >9,500 RNAs on the induction of HSC inactivation and identified ABHD17B as a potential target to inhibit liver fibrosis.

Results

Development of a high-throughput siRNA screening assay in primary human HSC-derived myofibroblasts

To identify gene products required for the maintenance of myofibroblast activity that could also serve as targets for antifibrotic drug development, we performed an siRNA screen of the human druggable genome in primary human HSC myofibroblasts. When cultured on plastic dishes, primary HSCs are activated and transdifferentiate into myofibroblasts[17,18]. Activated HSC-derived myofibroblasts can undergo inactivation, which is characterized by re-accumulation of lipid droplets in the cytoplasm and reduction of profibrotic markers such as *ACTA2* (encoding α-smooth muscle actin, α-SMA) and *COL1A1* (encoding the collagen type I alpha 1 chain)[15,16,19,20]. We previously developed high-throughput screening assays based on these characteristics and identified nortriptyline and nanchangmycin as antifibrotic compounds[21,22]. To take advantage of siRNA libraries to discover novel druggable targets with antifibrotic potential, we adapted our high-throughput lipid accumulation assay to be compatible with siRNA transfection. We optimized the reverse transfection protocol in primary human HSCs to achieve high transfection efficiency for siRNAs in 384-well format (**Supplementary Fig. 1A and 1B**).

Next, we evaluated negative and positive controls. We transfected HSCs with Dharmacon siGENOME non-targeting control siRNAs (NTC si) 1, 2, 3, 4 and 5, and performed Hoechst and Bodipy staining of the transfected cells to evaluate the effect of the siRNAs on lipid accumulation and cell number. Compared to NTC si1 and si2, HSCs transfected with NTC si3, si4, and si5 demonstrated lower percentages of Bodipy positive cells with similar or reduced effect on cell numbers (**Supplementary Fig. 1C-1D**). We then compared NTC si3-si5 negative control siRNAs with pooled siRNAs targeting *GAPDH* (*GAPDH* siP). We found that transfection with *GAPDH* siP did not cause a significant change in lipid accumulation (**Supplementary Fig. 1E**) and did not reduce cell numbers to the degree observed with non-targeting control siRNAs in the high-throughput format (**Supplementary Fig. 1F**). Based on these results, we chose *GAPDH* siP as our negative control.

We then evaluated potential siRNA positive controls for induction of lipid droplets and transfection efficiency. We tested pooled siRNAs targeting *ACTA2* and *ASAH1*[21] but depletion of these mRNAs did not significantly increase the percentage of Bodipy-positive cells (**Supplementary Fig. 1C**). Since efficient depletion of *PLK1* via siRNAs is established to cause cell death in multiple cell lines[23], we examined the possibility of using a reduction of cell number with siRNAs targeting *PLK1* as a proxy for transfection efficiency. Despite depletion efficiency for *PLK1* siRNAs of approximately 70%, the reduction in cell number was mild (~30%-40% decrease) (**Supplementary Fig. 1G and 1H**). These results showed that depletion of *ACTA2* or *ASAH1* did not affect lipid accumulation, and depletion of *PLK1* did not affect cell number sufficiently for these siRNAs to be used as controls in the assay.

To evaluate our screening approach and identify additional siRNA controls, we screened a pilot siRNA plate, composed of siRNA SMARTpools identified as hits in at least two different siRNA screens at the Institute of Chemistry and Cell Biology-Longwood (ICCB-L) (**Supplementary Fig.**

2A). We calculated the Z' factor for each plate based on the percent positive cells of nortriptyline[21] and *GAPDH* SMARTpool control wells and confirmed that the Z' was acceptable (0.4-0.5). From the pilot siRNA plate, we identified potential positive hits, including *AURKC*, *AKAP11*, and *TLR6* siRNAs (**Supplementary Fig. 2A**). We tested *AURKC*, *AKAP11*, and *TLR6* siRNAs, as well as *NFkB1*, *NFkB2*, *NR1H2* and *NR1H3* siRNAs, which are the annotated target genes shared by a few positive compound hits from our small molecule screen[22], for potential positive controls for the siRNA screen. Unfortunately, none of these siRNAs showed a sufficiently robust phenotype to be used as a positive control for Bodipy staining (**Supplementary Fig. 2B-J**). We did find that depletion of *UBB* dramatically reduced cell number (**Supplementary Fig. 2A**). We further validated that depletion of *UBB* significantly reduces HSC cell number in a dose-dependent manner (**Supplementary Fig. 3A-3B**). We tested the Z' of *UBB* siP versus *GAPDH* siP and nortriptyline versus *GAPDH* siP in at least 96 replicates and confirmed that the Z' values (0.25 and 0.60) were acceptable (**Supplementary Fig. 3C & 3D**). Thus, *UBB* pooled siRNA was used as a quality control for transfection efficiency and nortriptyline[21,22] as a positive control for Bodipy staining as a measure of HSC inactivation.

Primary siRNA screen in human HSC myofibroblasts identifies pooled siRNAs that inactivate HSC myofibroblasts

We next screened the Dharmacon SMARTpool siRNA library targeting a total of 7641 mRNAs from the human druggable genome as well as siRNAs targeting 2237 lncRNAs in a one target/well format. Each SMARTpool is composed equally of four duplexes targeting the same RNA. The screen was conducted in technical triplicate, with *GAPDH* SMARTpool siRNA as the negative control, *UBB* SMARTpool siRNA as the control for transfection efficiency, and 15 μM nortriptyline [21,22] as the control for lipid accumulation and Bodipy staining (**Fig. 1A-B and Supplementary Table 1**).

We adapted our previous analysis method[22] to calculate the score and toxicity for each siRNA pool. Briefly, the score was calculated based on the average percent Bodipy-positive cells for each siRNA pool compared to the baseline of the plate, as well as the correlation among the three replicates. Toxicity was calculated based on total cell numbers. There were a small fraction of outliers, possibly due to inefficient depletion for a replicate or artifacts acquired during image acquisition that impacted image analysis. Therefore, we developed a computational algorithm to correct outliers. Briefly, the interquartile range (IQR) was calculated for each SMART pool, and a cleaning parameter was set based on all IQRs observed in the screen, which was then applied to detect outliers. The values of the outliers were set to be the mean ± the cleaning parameter. This method allows us to retain variability while reducing the extreme variance that an outlying replicate can generate.

We identified 229 unique gene products as primary hits after screening the Dharmacon SMARTpool siRNA library in triplicate. This corresponded to 231 positive experimental wells in the primary screen because two wells contained the same siRNA pool, and one gene product was targeted by two different pooled siRNAs. We selected primary hits based on the following criteria: 1. the score is significantly increased (FDR < 0.05); 2. the toxicity is lower than the threshold determined by the nortriptyline wells; and 3a. transcripts per million (TPM) > 1 (for mRNAs) or TPM > 0.05 (for lncRNAs) in at least one of the 18 HSC RNA sequencing samples (Accession: GSE78853 and GSE68108)[21,24]; or 3b. no sequencing data were available in these analyzed datasets (**Fig. 1C and Supplementary Table 2**).

Secondary screen with individual siRNAs to validate gene targets that maintain HSC activation

As the primary screen was conducted with four siRNA duplexes pooled together in a one gene/well format, we next examined the phenotypic consequences of target depletion with individual duplexes in a one duplex/well, four wells/target format. This deconvolution secondary screen consisted of 920 experimental duplexes (targeting transcripts from 229 genes) tested in technical triplicate, relying on the same assay, controls, and analysis strategy as the primary screen (**Supplementary Table 3**). A total of 71 transcripts/gene products were validated as defined by at least two duplexes increasing Bodipy staining with an FDR < 0.05 and toxicity lower than the threshold determined by the *UBB* depletion (**Fig. 1D, and Supplementary Table 4**).

Screening for hits that regulate ACTA2 and COL1A1

When HSC myofibroblasts undergo inactivation, expression of *ACTA2* and *COL1A1* is reduced. In addition, the knockdown efficiency of an siRNA duplex is critical for the interpretation of the phenotype. Therefore, we sought to measure the mRNA levels of *ACTA2*, *COL1A1*, an internal housekeeping control, and the target mRNA for the 71 genes identified in the deconvolution screen.

To minimize technical variations, we measured *ACTA2*/*COL1A1*/target mRNA level in the same reaction as the housekeeping control *PSMB2* by performing multiplexed qRT-PCR with probes labeled with different dyes. *PSMB2* was selected as the reference mRNA because its expression shows minimal alteration during HSC inactivation[22]. In addition to the two duplexes with the highest scores in the deconvolution screen, we also included three additional siRNA duplexes from the Ambion siRNA library for 70 of the genes (one of the 71 genes was not covered by the Ambion siRNA library). A total of 352 siRNA duplexes were tested by qRT-PCR in quadruplicate.

We analyzed mRNA expression results for *ACTA2/PSMB2 and COL1A1/PSMB2* using two methods: a linear regression method and the standard ΔΔCt method. Depletion of each target transcript was also calculated using the standard ΔΔCt method with *PSMB2* as the endogenous control (**Supplementary Table 5**). We observed that *COL1A1* reduction does not always correlate with *ACTA2* reduction. Approximately 66% of the siRNA duplexes were confirmed to have a knockdown efficiency of greater than 50%, and approximately 69% of the siRNA duplexes reduced the expression of the target transcript by more than 40%. The knockdown efficiency of 11% of siRNA duplexes could not be determined due to low expression of the target transcript or low-quality melting curves (**Fig. 1E**). We further prioritized the siRNA screen candidates based on the following criteria: **priority 1**: at least two siRNAs reduced *COL1A1* by at least 30% (based on the fold change calculated either by the linear regression strategy or the ΔΔCt method) with at least 40% depletion of the target gene; **priority 2**: at least three siRNAs reduced *ACTA2* by at least 60% (based on the fold change calculated either by the linear regression strategy or the ΔΔCt method) with at least 40% depletion of the target gene; **priority 3**: at least two siRNAs reduced *ACTA2* by at least 60% (based on the fold change calculated either by the linear regression strategy or the ΔΔCt method) with at least 40% depletion of the target gene. In total, we identified 23 genes as priority 1-3 candidates, including eleven genes at priority 1, four genes at priority 2, and eight genes at priority 3 (**Fig. 1F** and **Table 1**).

Of note, 37 lncRNA genes were among the 230 hits of the primary screen, and three lncRNA genes (*AK2*/NR_037592, *C1orf140*/NR_024236, and *CLTB*/NR_045724) were among the 71 hits of the deconvolution screen. Depletion of these three lncRNA genes had some effect on *ACTA2* but did not reduce *COL1A1* mRNA levels, and no lncRNA genes were ranked as priority 1-3 candidates.

ABHD17B depletion increases lipid accumulation and reduces HSC activation

After evaluating the priority 1 candidates, *ABHD17B* was selected for further characterization. *ABHD17B* encodes an enzyme with palmitoyl-hydrolase activities, which hydrolyzes fatty acids from S-acylated cysteine residues and regulates the palmitoylation of proteins including N-Ras [25]. First, we confirmed the effect of *ABHD17B* knockdown on lipid accumulation using primary HSCs from multiple human donors. Transfection with two different *ABHD17B* siRNA duplexes significantly increased the accumulation of lipid droplets in cells from three different donors. HSCs from the remaining donor (donor 2) showed a significant increase in lipid accumulation with one *ABDH17B* siRNA, while the other siRNA did not have a significant effect (**Fig. 2A**). Transfection with an siRNA targeting UBB was also included in this experiment to confirm transfection efficiency. These results confirm that depletion of *ABHD17B* is sufficient to increase lipid accumulation, which suggests an inactive HSC phenotype.

Consistent with the screening results in HSCs from donor 1 (**Fig. 1**), the depletion of *ABHD17B* reduced *ACTA2*, *COL1A1* and *COL3A1* levels in HSCs from donor 3 two days after transfection (**Fig. 2B**). Next, we tested if depletion of *ABHD17B* affects the formation of α-SMA fibers as a marker of HSC activation and collagen deposition in the ECM as an indication of fibrotic activity. Compared to non-targeting control siRNAs (NTC siP and NTC si5), both the siRNA pool (siP) and two different siRNA duplexes targeting *ABHD17B* significantly reduced *ABHD17B* mRNA in HSCs from two different donors (**Fig. 2C**), without affecting cell number (**Supplementary Fig. 4A**). Consistent with the described effects on *ACTA2* and *COL1A1* transcripts (**Fig. 2B**), ABHD17B depletion resulted in reduced HSC activation as evident from reduced staining of α-SMA (encoded by *ACTA2*) and collagen type I (**Fig. 2D-2G, Supplementary Fig. 4B and 4C**). Two positive controls, siRNAs targeting *TGFBR1* and *ACTA2* were also included. The observed effect of

ABHD17B depletion on HSC phenotype suggests that ABHD17B promotes maintenance of myofibroblast features.

ABHD17B promotes collagen expression in lung fibroblasts

Similar to liver fibrosis, idiopathic pulmonary fibrosis (IPF) is characterized by excessive ECM synthesized by activated fibroblasts and has very limited treatment options[26–28]. Since depletion of *ABHD17B* induces inactivation of HSCs, we asked if ABHD17B also plays a role in promoting the fibrotic activity of primary human lung fibroblasts. We found that depletion of *ABHD17B* significantly reduced the expression of *COL1A1* and *ACTA2* (**Supplementary Fig. 5**), indicating that ABHD17B also plays a role in regulating the fibrotic activity of primary human lung fibroblasts.

ABHD17B and ABHD17C promote collagen expression in HSCs

ABHD17B belongs to the ABHD17 family, which includes two additional serine hydrolase proteins, ABHD17A and ABHD17C. All three family members are expressed in primary human HSCs, as indicated by RNA sequencing data[21,22], and we found that depletion of *ABHD17B* and depletion of *ABHD17C* are each associated with reduced *COL1A1* expression in the three primary HSC donor lines tested, while depletion of *ABHD17A* was associated with modest reduction of *COL1A1* in one line and no significant change in the other two lines (**Fig. 2H**). We next evaluated the effect of depletion of each ABHD17 family member on expression of other family members (**Supplementary Fig. 6A-C**). Depletion of *ABHD17B* did not affect *ABHD17A* or *ABHD17C* expression except for a small decrease in *ABHD17A* observed in one line. Depletion of *ABHD17C* showed a small decrease in *ABHD17A* in one line, while siRNAs targeting *ABHD17A* were associated with a small increase in *ABHD17B* in two lines and a decrease in ABDH17*C* three

lines. The overall findings suggest that both *ABDH17B* and *ABHD17C* can promote *COL1A1* expression, and depletion of *ABHD17B* has minimal effect on the expression of other family members.

Analysis of ABHD17B structure

ABHD17 family proteins were identified as depalmitoylases in a screen for serine hydrolases that increase the turnover of palmitate[25]. ABHD17A has the strongest depalmitoylase activity, which was shown to be mitigated with a Ser to Ala mutation[25]. We performed structural analysis of ABHD17B with molecular dynamics (MD) simulations following *de novo* folding with AlphaFold[29] (**Supplementary Fig. 7A)** [29]**.** Structural analysis of ABHD17B identified Ser170 on a loop between an alpha helix and beta sheet proximal to Asp235. His264 is located on a second loop between a different alpha helix and beta sheet, capable of forming a catalytic triad representative of alpha beta hydrolases (**Supplementary Fig. 7B-D**)[30]. These findings suggested that Ser170 has a high likelihood of being the active residue for depalmitoylation and that mutation of this residue would disrupt depalmitoylase activity. We performed a serine activity based probe assay (SABP) to quantify the activity of WT ABHD17B and ABHD17B containing a Ser to Ala mutation at residue 170 (S170A) and found that the mutation resulted in reduced hydrolase activity (**Fig. 3A**). These findings indicate that S170 is required for normal serine hydrolase/depalmitoylase activity in ABHD17B.

Next we asked how the S170A mutation affected *COL1A1* expression in HSCs. Ectopic expression of WT ABHD17B was associated with an increase in *COL1A1* expression (**Supplementary Fig. 8A and 8B**), and ectopic expression of WT ABHD17B (**Supplementary Fig. 8C)** produced significantly higher levels of *COL1A1* than expression of ABHD17B-S170A

(**Fig. 3B**). These results suggest that S170 may be required for ABHD17B to promote *COL1A1* expression.

Depalmitoylase activity of ABHD17B is not required to promote HSC activation

The decrease in *COL1A1* expression with ectopic expression of ABHD17B-S170A compared to WT ABHD17B suggested that depalmitoylation activity of the serine protease pocket may be required to promote the fibrotic activity of HSCs. We treated HSCs with increasing concentrations of the depalmitoylase inhibitor Palmostatin B (PalmB)[25] (**Fig. 3C**) [25]. Following PalmB treatment, a modest increase of lipid droplets was observed only at the highest concentration of 100 μM, while there was no difference at lower concentrations. Similar results were observed in all four HSC lines tested (**Fig. 3C**). We next evaluated the effect of the depalmitoylase inhibitor ABD957[31]. We confirmed activity of the inhibitor (**Supplementary Fig. 8D**), but even at concentrations up to 30 μM, ABD957 had no effect on lipid accumulation in HSCs (**Fig. 3D**) and did not reduce *ACTA2* or *COL1A1* expression (**Fig. 3E**). These results showed that global inhibition of depalmitoylase activity does not affect the fibrotic activity of HSCs.

ABHD17 proteins regulate NRAS palmitoylation and NRAS subcellular localization[25], and NRAS has been linked to fibrotic diseases such as idiopathic pulmonary fibrosis (IPF)[32]**.** To further evaluate whether the depalmitoylase activity of ABDH17B might affect the fibrotic activity of HSCs through this pathway, we asked if depletion of NRAS affects *ACTA2* and *COL1A1* expression. We found that depletion of NRAS in two HSC lines did not significantly affect *COL1A1* expression, and the effect on *ACTA2* was variable over time points and cell lines (**Fig. 3F**). These findings suggest that ABHD17B regulates *COL1A1* through a process independent of NRAS.

Analysis of global gene expression and interacting partners

We next performed RNA sequencing (RNA-seq) and differential expression analysis to define genes and pathways affected by depletion of ABHD17B. ABHD17B was depleted with two different siRNA duplexes, and each was compared to the nontargeting control (NTC) (**Supplementary Table 6**). Results from both analyses were combined, which showed that depletion of *ABHD17B* was associated with a decrease in expression of genes involving the cytoskeleton, adhesion, contractility, ECM, and spindle formation (**Fig. 4A and Supplementary Fig. 9**). Heatmaps are shown for genes associated with these Gene Ontology (GO) categories to highlight the mRNAs most affected by depletion of *ABHD17B* (**Fig. 4B and Supplementary Fig. 10**). These results suggest that ABDH17B promotes expression of genes regulating HSC contractility, adhesion, and ECM production to drive fibrosis.

We then evaluated the protein partners of ABHD17B. We ectopically expressed ABHD17B-FLAG and control GFP-FLAG in HSCs before performing precipitation with M2 beads followed by mass spectrometry (MS). The proteins showing the strongest enrichment with ABHD17B precipitation **(Supplementary Table 7, bold)** are enriched in pathways (**Fig. 4C**) that are similar to the pathways affected by depletion of *ABHD17B* (**Fig. 4A**). We next evaluated interactions between the 15 proteins showing the strongest interaction with ABHD17B (**Fig. 4D**). One large cluster is identified in which proteins are linked by experimental data supporting their interaction (red lines), while a second cluster contains the serine/threonine kinases STK38 and STK38L. ABDH17B is also included in this network analysis, but there was no previous evidence of interaction. Together, RNA-seq and MS data indicate that ABHD17B promotes expression of gene products involved in cytoskeletal organization, contractility, adhesion, and ECM, and ABHD17B also directly interacts with proteins in these pathways.

Loss of Abhd17b protects against the development of liver fibrosis in a carbon tetrachloride model

Abhd17b+/- mice were intercrossed, and *Abhd17+/+, Abhd17+/-*, and *Abhd17b-/-* offspring were generated in expected Mendelian ratios (not shown). *Abhd17b-/-* mice bred normally, and liver histology appeared no different than that of *Abhd17b+/+* mice (**Fig. 5A**). Mice were then treated with carbon tetrachloride (CCl_4) by oral gavage to induce liver fibrosis. Mice deficient in *Abhd17b* showed reduced fibrosis as measured by hydroxyproline (**Fig. 5B**) and collagen proportionate area (**Fig. 5C, D**). These results suggest that Abhd17b is necessary for a robust fibrotic response in the setting of chronic liver injury.

Discussion

Extent of fibrosis remains the strongest predictor of liver-related mortality in the setting of chronic liver disease[33,34]. While treating the underlying causes of liver injury have been successful in halting progression and even promoting regression of fibrosis[1,2], effective treatments are not available for many sources of disease[3,4,6]. HSC activation and transdifferentiation into HSC myofibroblasts as a result of chronic injury is the primary process leading to accumulation of collagen and other components of the ECM that form the fibrotic scar[9–11]. Here, we performed an siRNA screen to identify gene products necessary to maintain the fibrotic phenotype of HSC myofibroblasts, with the goal of defining new therapeutic targets to inhibit fibrosis. We screened siRNAs targeting >9,500 RNAs applying a phenotypic readout in the primary screen, quantifying accumulation of lipid droplets to mark HSC inactivation. We then evaluated expression of genes that mark fibrosis (*COL1A1*) and HSC activation (*ACTA2*) in a secondary screen. This analysis identified 23 genes as high priority, and we focused on the activity of ABHD17B. In addition to promoting the fibrotic activity of HSCs, we also found that ABHD17B promotes *COL1A1*

expression in pulmonary fibroblasts, and the antifibrotic effects of *ABHD17B* depletion may also extend to depletion of *ABHD17C*.

ABHD17B is a member of the ABHD17 family of proteins, which have depalmitoylase activity [25,31]. Through structural analysis we predicted that Ser 170 is the active residue for serine protease activity of ABHD17B, and mutation of this residue confirmed this prediction. However, our data suggest that the depalmitoylase activity of ABHD17B is not required for its profibrotic function. Treatment of HSCs with two different inhibitors of depalmitoylase activity had no effect on *COL1A1* expression in HSCs. Further, depletion of NRAS, a primary target of ABHD17 family depalmitoylation, also had no effect on collagen expression in HSCs. We did observe that the S170A mutation decreased the ability of ABHD17B to promote *COL1A1* expression, raising the possibility that this mutation may have other effects on the structure of ABHD17B or may affect intracellular localization or levels of ABHD17B protein.

RNA-seq and MS studies were performed to better understand how ABHD17B may function independent of depalmitoylation/serine hydrolase activity. RNA-seq showed that ABHD17B affects the expression of genes that control cytoskeleton, adhesion, interface with the ECM, and contractility. MS studies showed that ABHD17B associates with proteins that are primarily cytoplasmic and involved in pathways of actin binding/assembly, cell adhesion, and cadherin binding. The largest cluster (Fig. 4D) contains actin subunits, capping proteins, and myosin motors involved in contractility. CAVIN1/PTRF is not part of any cluster, but in addition to a role in dissociating the polymerase I complex to terminate transcription[35], it is also part of the caveolin complex[36], which regulates actin cytoskeleton and adhesion in HSCs[37]. There are multiple nuclear functions attributed to HNRPNK, including regulation of RNA splicing, RNA stability, and transcription[38–41], but it is also found in the cytoplasm associated with calponin[42,43], a protein that binds actin as part of a complex regulating contractility[44]. STK38

and STK38L (NDR1/2) are serine-threonine kinases that form a separate cluster. These proteins are related to LATS1/2 in the HIPPO signaling pathway[45], and STK38 regulates MHY6 and sarcomere assembly in cardiomyocytes[46], suggesting that it could modulate other conventional non-muscle myosin in fibroblasts. The source of interaction with mitochondrial proteins (ATP5a1) is unclear but is linked to MHY9 (**Fig. 4D**). While the interactions with individual proteins need to be validated, the combination of interacting partners identified by MS suggests ABHD17B may regulate HSC activity by modifying the actin cytoskeleton and regulating contractility, thereby affecting how HSCs sense and respond to the stiffness of their environment. These conclusions fit with the observed decrease in activation and collagen expression in HSCs and other fibroblasts cultured in a soft matrix and the links between the actin cytoskeleton and collagen expression[47–52] and suggest ABHD17B could also affect contraction and migration.

In summary, we performed an siRNA screen to identify genes that promote a fibrotic phenotype in primary human HSCs, leading to the identification of ABHD17B as a target to inhibit liver fibrosis. Depletion of *ABHD17B* in primary HSCs decreases *COL1A1* mRNA and collagen protein levels, and modulates pathways involving the actin cytoskeleton, contractility, focal adhesion, and ECM based on RNA-seq and MS analysis. Furthermore, mice deficient in Abhd17b are protected from liver fibrosis. These findings suggest that targeting ABHD17B-dependent pathways in HSCs may be a viable approach to reduce fibrosis. However, current small molecules inhibiting the depalmitoylase activity of ABHD17B do not affect this process. Further studies will be required to advance approaches to inhibit the pro-fibrotic activity of ABDH17B, including discovery of new small molecules targeting ABDH17B or development of modified antisense oligonucleotides[53] to deplete ABDH17B.

Materials and methods

Animals

All mouse experiments were approved by the IACUC of the Massachusetts General Hospital (2017000074). *Abhd17b+/-* (*C57BL/6N-Abhd17b*$^{em1(IMPC)J}$*/Mmucd*) mice were purchased from the Mutant Mouse Resource and Research Center (MMRRC) and were maintained on C57BL/6 background. Male mice received 40% carbon tetrachloride (CCl_4) diluted in olive oil or olive oil control by oral gavage (100 μl total volume) three times a week for four weeks[54]. *Abhd17b-/-* and *Abhd17b+/+* mice were generated from *Abhd17b-/-* and *Abhd17b+/+* siblings produced from *Abhd17b+/-* parents. Studies were initiated on age matched *Abhd17b-/-* and *Abhd17b+/+* mice at 8-9 weeks of age.

Cell culture and compound treatments

The primary human hepatic stellate cells (HSCs) were cultured as described previously[22]. Donor information is provided below.

Donor	Vendor ID	Age	Gender	Race	BMI
1	Lonza, HUCNP, ID: 4105	45	M	Caucasian	24.2
2	Lonza, HUCNP, ID: 4270	35	M	Caucasian	42.1
3	Lonza, HUCLS, ID:180761	57	F	African American	48.8
4	Lonza, HUCLS, ID: 182821	24	F	African American	24.5
5	Tebubio (source: Zen-Bio), HP-F-S	48	M	Caucasian	33
6	Tebubio (source: Zen-Bio), HP-F-S	38	M	African American	18

Primary lung fibroblasts were collected from deidentified discarded excess tissue (donor 699) through the MGH Fibrosis Translational Research program and cultured as described previously[28].

Palmostatin B was purchased from Calbiochem (Cat. # 178501). ABD957 was synthesized by chemists from BI (purity: 93% as determined by HPLC-MS; MS (ESI^+): m/z = 628.6 $[M+H]^+$, 628.2 calculated). Nanchangmycin was purchased from Adooq (Cat. # A10621). Nortriptyline was purchased from Sigma (Cat. # N7261). HSCs were treated with compounds for 48 hr at concentrations as indicated before cells were fixed or lysed.

Reverse transfection of siRNAs in the screen and follow-up experiments

For the screening, transfection was performed in 384-well plates (Corning, Cat. # 3764) in a high-throughput manner using Bravo Automated Pipettor (Agilent) and Multidrop Combi Reagent Dispenser (Thermo Fisher Scientific). For each well in a 384-well plate, 1.25 μL siRNAs (in 1 μM stocks) were diluted in 8.5 μL Opti-MEM (to make the final concentration of 25 nM) in the wells, and then 10 μL diluted Dharmafect-1 (Horizon Discovery, Cat. # T-2001-02, 9.95 μL Opti-MEM + 0.05 μL Dharmafect-1) was added. After a 40 min incubation, 750 HSCs in 30 μL antibiotics-free transfection media (DMEM + 16% FBS) were added to the siRNA and Dharmafect-1 mixture in each well. Cells were fixed and stained with Bodipy and Hoechst at 72 hr after transfection. The siRNAs used in the screen and the siRNAs targeting *FAM160B2*, *MGAT5B*, *TMEM134*, *TTTY2* and *TTY2B* were provided by the Institute of Chemistry and Cell Biology (ICCB)-Longwood screening facility, and the relevant information is provided in the supplementary tables and in the table below.

Gene Symbols	Accession Numbers	si	Sequence	Anti-sense Sequence
FAM160B2	NM_022749	1	GGAGACAGGCUAUGACACA	UGUGUCAUAGCCUGUCUCC
		2	GCAGAGAAUCCAGAGGGUA	UACCCUCUGGAUUCUCUGC
		3	GGCAUCAGCUGGAGGUUAC	GUAACCUCCAGCUGAUGCC
		4	CCGAGAUCGUCAACAGUUU	AAACUGUUGACGAUCUCGG
MGAT5B	NM_144677	1	GGACGGAACCUGCGUACAA	UUGUACGCAGGUUCCGUCC
		2	CAAGUUCCCUGACUGCUCA	UGAGCAGUCAGGGAACUUG
		3	GAACGUCUCCGACAUCGCU	AGCGAUGUCGGAGACGUUC
		4	GGACAGUCGACUACAACAA	UUGUUGUAGUCGACUGUCC
TMEM134	NM_001078650	1	CAACACCCUUUGAUCCAGA	UCUGGAUCAAAGGGUGUUG
		2	CCUGGAGUCUAUCACGUGA	UCACGUGAUAGACUCCAGG
		3	GGUUCGAGGUGGCUGACGA	UCGUCAGCCACCUCGAACC
		4	AUUAAUUCCACCAGAGGCA	UGCCUCUGGUGGAAUUAAU
TTTY2	NR_001536	1	GGUCAAUAAUUUUACGGUA	UACCGUAAAAUUAUUGACC
		2	CCUAUUAAAUUUACCUCGA	UCGAGGUAAAUUUAAUAGG
		3	UGAGAGACCCGUUCGACAU	AUGUCGAACGGGUCUCUCA
		4	CCCCAGGAAUAAACGGCAA	UUGCCGUUUAUUCCUGGGG
TTTY2B	NR_003590	1	GGUCAAUAAUUUUACGGUA	UACCGUAAAAUUAUUGACC
		2	CCUAUUAAAUUUACCUCGA	UCGAGGUAAAUUUAAUAGG
		3	UGAGAGACCCGUUCGACAU	AUGUCGAACGGGUCUCUCA
		4	CCCCAGGAAUAAACGGCAA	UUGCCGUUUAUUCCUGGGG

For validation experiments, the transfection in HSCs was scaled up to 96-well plates (for staining) and 12-well plates (for qRT-PCR) proportionally based on surface area from the protocol described above. Various RNA concentrations were used as indicated in the figures and legends. For transfection of siRNAs in primary lung fibroblasts, cells were reverse transfected using lipofectamine 2000 (Thermo Fisher Scientific, Cat. # 11668019) according to manufacturer's

manual at 5000 cells/cm^2 with 20 μM siRNA. Cells were fixed or lysed 72 hr after transfection unless indicated otherwise in the legends. The siRNAs used in the validation experiments were purchased from Horizon Discovery as listed below.

Full name	**Abbreviation**	Cat. #
siGENOME non-targeting control siRNA#1	NTC si1	D-001210–01
siGENOME non-targeting control siRNA#2	NTC si2	D-001210–02
siGENOME non-targeting control siRNA#3	NTC si3	D-001210–03
siGENOME non-targeting control siRNA#4	NTC si4	D-001210–04
siGENOME non-targeting control siRNA#5	NTC si5	D-001210–05
siGENOME human *ACTA2* siRNA 1	*ACTA2* si1	D-003450-01
siGENOME human *ACTA2* siRNA 2	*ACTA2* si2	D-003450-02
siGENOME human *ASAH1* siRNA 1	*ASAH1* si1	D-005228-01
siGENOME human *ASAH1* siRNA 4	*ASAH1* si4	D-005228-04
siGENOME human *PLK1* SMARTpool	*PLK1* siP	M-003290-01
siGENOME human *KIF11* SMARTpool	*KIF11* siP	M-003317-01
siGLO RISC-free siRNA	siGLO	D-001600-01
siGENOME human *GAPDH* SMARTpool	*GAPDH* siP	M-004253-02
siGENOME human *NFkB1* SMARTpool	*NFkB1* siP	M-003520-01
siGENOME human *NFkB2* SMARTpool	*NFkB2* siP	M-003918-02
siGENOME human *NR1H2* SMARTpool	*NR1H2* siP	M-003412-03
siGENOME human *NR1H3* SMARTpool	*NR1H3* siP	M-003413-01
siGENOME human *UBB* SMARTpool	*UBB* siP	M-013382-01
siGENOME human *TLR6* SMARTpool	*TLR6* siP	M-005156-01
siGENOME human *AURKC* SMARTpool	*AURKC* siP	M-019573-04
siGENOME human *AKAP11* SMARTpool	*AKAP11* siP	M-009277-01

siGENOME human *ABHD17B* siRNA#1	*ABHD17B* si1	D-005809-01
siGENOME human *ABHD17B* siRNA#4	*ABHD17B* si4	D-005809-04
siGENOME human *NRAS* SMARTpool	*NRAS* siP	M-003919-00
siGENOME human *ABHD17A* SMARTpool	*ABHD17A* siP	M-005947-02
siGENOME human *ABHD17C* SMARTpool	*ABHD17C* siP	M-005929-02
ON-TARGETplus human ABHD17B pool	ABHD17B siP	L-005809-01
ON-TARGETplus non-targeting control pool	NTC siP	D-001810-10

Lipid accumulation assay based on Hoechst and Bodipy staining

HSCs transfected with siRNAs or treated with compounds were fixed with 4% paraformaldehyde (Electron Microscopy Sciences, Cat. # 15710) for 15 min at room temperature (RT). Cells were washed with DPBS and stained with Bodipy 493/503 (0.25 µg/mL, Invitrogen, Cat. # D3922) and Hoechst (5 µg/ mL, Invitrogen, Cat. # H1399) for 45 min at RT. Images were taken with the ImageXpress Micro Confocal (Molecular Devices) at the Institute of Chemistry and Cell Biology (ICCB)-Longwood screening facility and analyzed using the MetaXpress software. Cells with a cytoplasmic Bodipy staining intensity higher than the cutoff were defined as Bodipy-positive cells. Cells were counted and normalized to the total nuclei count in the same microscopic field to calculate the percentage of Bodipy positive cells. The cutoff was adjusted for each plate, so that there are about 10-20% Bodipy-positive cells in the DMSO condition and 80-90% Bodipy-positive cells in the nortriptyline-treated positive control wells. For the primary screen, the results were scanned for outliers, which were then corrected based on the method described below. The score was then calculated based on the averaged percent positive cells for the siRNA compared to the baseline of the plate, as well as the correlation among three replicates. Toxicity was calculated based on total cell numbers.

Outlier correction in the primary and validation screens

To determine if the replicates of a specific library well contain outliers, the interquartile range (IQR) was calculated using all the replicates for each siRNA. The minimum IQR that was considered an outlier among all IQRs was used to set up the threshold to correct for outliers. In the primary screen, siRNAs that had an IQR larger than 11.3891 were corrected. To correct an outlier, the Tukey's method was applied, which uses a cleaning parameter to detect outliers. The cleaning parameter is 1.5 x 11.3891, following the same logic as the outlier detection when plotting a boxplot. If any value was larger than the median +/- the cleaning parameter, that value was set to be exactly the median +/- the cleaning parameters. This method allows us to keep some of the variability while reducing the extreme variance that an outlier can generate.

High-throughput evaluation of mRNA expression and knockdown efficiency

HSCs were transfected with siRNAs as described above. 72 hr after transfection, cells were harvested using the Cells-to-CT 1-Step Taqman Kit (Invitrogen, Cat. # A25603) as previously described[22] except that lysis was performed with 15 µL lysis buffer (plus DNase) for 5 min at RT, and then the reaction was stopped by adding 1.5 µL stop solution and incubating for 2 min at RT. To quantify the depletion of each target gene, customized 384-well plates arrayed with Taqman probes for each mRNA target gene were purchased from Thermo Fisher Scientific. Reverse transcription and amplification of cDNA was performed with Taqman 1-Step qRT-PCR mix supplied with the kit. *ACTA2*, *COL1A1* and target mRNA were each quantified in the same well with the endogenous control *PSMB2*. *ACTA2*, *COL1A1*, and target mRNA Taqman probes are FAM-labeled, while the *PSMB2* probe is VIC-labeled and primer-limited.

mRNA expression analysis in screen

The mRNA expression results for *ACTA2* (normalized to *PSMB2*) and *COL1A1* (normalized to *PSMB2*) were analyzed using two methods: the linear regression strategy and the standard ΔΔCt method. For the linear regression strategy, the data was fit to a linear model: Ct_*ACTA2* (or *COL1A1*) ~ Ct_*PSMB2* + plate + siRNA. The estimate for each experimental siRNA was compared to that of the control siRNA to calculate the relative fold change. The knockdown efficiency for each target gene was calculated using the standard ΔΔCt method with *PSMB2* as the endogenous control.

qRT-PCR analysis

RNA samples were extracted using TRIzol (Invitrogen, Cat. # 15596026). Using 1 µg total RNA as input, reverse transcription was performed with the iScript gDNA Clear cDNA Synthesis Kit (BIO-RAD, Cat. # 1725035) according to manufacturer's instructions. TaqMan Universal PCR Master Mix (Applied Biosystems, Cat. # 4305719) and TaqMan Real-time PCR Assays (Thermo Fisher Scientific) were used for the quantitative real-time PCR analysis of the cDNA samples. For each qRT-PCR experiment, each dot represents the mean value for a single sample analyzed in duplicate to quadruplicate and *PSMB2* as the endogenous control[22]. For Supplemental Fig. 8A and 8B, four independent experiments were combined and included all samples in which transduction with ABHD17B-FLAG lentivirus induced *ABDH17B* mRNA by at least 3 fold. The gene-specific TaqMan Real-time PCR Assays used in this study are listed below.

	Assay ID
Human *ACTA2*	Hs00426835_g1

Human *COL1A1*	Hs00164004_m1
Human *PSMB2*	Hs01002946_m1
Human *ASAH1*	Hs00602774_m1
Human *PLK1*	Hs00983227_m1
Human *UBB*	Hs00430290_m1
Human *ABHD17B*	Hs00925211_m1
Human *GAPDH*	Hs02786624_g1
Human *NRAS*	Hs00180035_m1
Human *COL3A1*	Hs00943809_m1
Human *ABHD17A*	Hs07290154_g1
Human *ABHD17C*	Hs01593305_m1
Human *AURKC*	Hs00152930_m1
Human *AKAP11*	Hs01568654_m1
Human *TLR6*	Hs04975840_m1
Human *NFkB1*	Hs00765730_m1
Human *NFkB2*	Hs01028890_g1
Human *NR1H2*	Hs01027208_m1
Human *NR1H3*	Hs00172885_m1

Generation of ABHD17B S170A mutant

DNA sequences that encode the wildtype amino acid sequence of human *ABHD17B* and encode a mutation of Ser 170 to Ala in *ABDH17B* were synthesized by GENScript. The cDNAs also

contain identical additional nucleotide modifications that do not affect amino acid sequence (**Supplementary Fig. 11**).

Analysis of α-SMA fibers and extracellular collagen deposition (scar-in-a-jar assay)

Primary human HSCs were seeded in 384-well plates (CellCarrier-384 Ultra plates, Cat. # 6057300) in stellate cell medium (ScienCell/Innoprot, Cat. # 5301-b) supplemented with 2% FCS (Thermo Fisher Scientific), 1% penicillin/streptomycin, and stellate cell growth supplement (ScienCell/Innoprot, Cat. # 5352), and transfected using JetPrime transfection reagent (Polyplus, Cat. # 101000027). The final siRNA concentration per well was 16 nM with 0.8 µl transfection reagent per well. Cells were serum starved the next day, followed by stimulation with TGF-β (10 ng/ml, R&D, Cat. # 240-B) in conditions of molecular crowding (37.5 mg/ml Ficoll 70 and 25 mg/ml Ficoll 400, GE Healthcare, Cat. # 17-0310-10 and # 17-0300-10) and vitamin C supplementation (0.2 mM; Sigma, Cat. # A8960) to promote collagen deposition. 72 hr post TGF-β stimulation, cells were fixed in 80% Methanol for 30 min, washed in PBS, and permeabilized using 1% TritonX 100 in PBS. Cells were blocked in 3% BSA for 30 min at RT and incubated with anti-alpha-SMA antibody (1:1000; Sigma, Cat. # A2547) and anti-collagen type I antibody (1:1000; Sigma, Cat. # SAB4200678) in PBS at 37° C for 1.5 hr. Cells were washed with PBS and incubated with secondary antibodies for 30 min at 37° C (1:1000 AF568 goat anti-mouse IgG1 Thermo Fisher Scientific, Cat. # A-21124; and 1:1000 AF647 goat anti-mouse IgG2a Thermo Fisher Scientific, Cat. # A-21241). Nuclei were stained with Hoechst (1 µM, Molecular Probes, Cat. # H-3570), cells with HSC Cellmask GreenTM at 0.2 µg/ml (Invitrogen, Cat. # H32714). Nuclear, cytoplasm, αSMA and collagen-I images were acquired using the IN Cell Analyzer 2200, images transferred to Perkin Elmer's Columbus Image Storage and Analysis system, and

analyzed using a custom image analysis protocol with total cell number, number of aSMA fibers/cell, and collagen area/total cell number being quantified, as described[55].

For quantification of siRNA-mediated silencing, cells were transfected and treated as described above, lysed in RLT Plus buffer, and RNA isolated with the RNeasy Plus Kit according to the manufacturer's protocol (Qiagen, Cat. # 74134). To obtain sufficient material for qRT-PCR, lysates from 6-12 wells were pooled prior to RNA isolation. 150 ng RNA were reverse transcribed using the High-capacity cDNA Archive Kit (Applied Biosystems, Cat. # 4322169) and Taqman assays performed using TaqMan Universal PCR Master Mix (Applied Biosystems, Cat. # 4318157), probes listed in the table above, and the ViiA 7 Real-Time PCR System (Thermo Fisher Scientific).

Pulmonary fibroblast analysis

Primary human lung fibroblasts were seeded in 96-well plates at $1.6X10^3$ cells/well, reverse transfected with 20 nM pooled siRNAs targeting *ABHD17B* (si1 and si4 mixed at 1:1) per well in duplicates in 12.5% FBS without antibiotics. After 48 hr, cells were changed to serum free media. After serum starvation for 24 hr, cells were treated with or without 10 ng/ml TGFβ (R&D Systems, Cat. # 240-B) for another 24 hr and harvested for RNA extraction after 72 hr.

Serine activity probe based assays

Thermo Scientific™ ActivX™ Desthiobiotin-FP Serine Hydrolase Probe was purchased from Thermo Fisher (Cat. # 88317). Anti-FLAG® M2 Magnetic Beads (Cat. # M8823-1ML) were purchased from Milipore Sigma. Blots were developed with either anti-biotin, HRP-linked antibody (Cell Signaling, Cat. # 7075), streptavidin (SA) HRP (Cell Signaling, Cat. # 3999) or anti-FLAG

antibody (Cell Signaling, Cat. # 14793). HEK-293T cells were transiently transfected using X-tremeGENE™ 9 DNA Transfection Reagent (Roche, Cat. # XTG9-R0) with 6 µL of transfection reagent to 2 µg plasmid for 48 hr. Cells were harvested in 300 µL Pierce™ IP Lysis Buffer (Thermo Scientific, Cat. # 87787) and frozen at -80° C. Lysates were cleared at 10,000 *g,* and an equal amount of equilibrated Millipore Sigma Anti-FLAG® M-2 Magnetic Beads (Cat. # M8823) in Pierce Lysis Buffer was added, followed by 2 washes in 1 mL Pierce Lysis Buffer using magnetic rack. Beads were resuspended in 50 µL of Pierce Lysis Buffer and labeled with addition of 1 µL of ActivX™ Desthiobiotin-FP stock (at 100 µM in DMSO) for 30 min on bead, rocking at RT with occasional vortexing. NuPAGE™ Sample Reducing Agent (10X) (Invitrogen, Cat. # NP0009) and NuPAGE™ LDS Sample Buffer (4X) (Invitrogen, Cat. # NP 0007) were added to samples before boiling at 95 °C for 5 min. Samples were loaded on Bolt™ 4 to 12%, Bis-Tris, 1.0 mm, Mini Protein Gels (Cat. # NW04120BOX) in NuPAGE™ MOPS SDS Running Buffer (20X) (Cat. # NP 0001002). SeeBlue™ Plus2 Pre-stained Protein Standard (Cat. # LC5925) was used as a molecular weight marker. After electrophoresis, material was transferred to iBlot™ 2 Transfer Stacks, nitrocellulose (Cat. # IB23001) using an iBlot™ 2 Gel Transfer Device (Cat. # IB21002S). Nitrocellulose was blocked in 1% BSA (Thermo Scientific, Cat. # 37520) and probed using anti-biotin antibody or SA-HRP overnight at 4 °C. Blots were washed 3 times with Tris Buffered Saline-Tween (TBST) buffer (Boston BioProducts, Cat. # IBB-181–6) and developed using SuperSignal™ West Pico PLUS Chemiluminescent Substrate (Thermo Scientific, Cat. # 34580). Blots were then stripped according to manufacturer's specifications with Thermo Fisher Scientific Restore™ Western Blot Stripping Buffer (Cat. # 21059), washed in TBST 3 times, re-blocked in 1% BSA and re-probed with anti-FLAG antibody overnight at 4° C. Nitrocellulose was then washed 3 times in TBS-T and probed with goat-anti- anti-Rabbit IgG (H+L) secondary antibody, HRP (Invitrogen, Cat. # 34260).

Protein Structure Prediction for ABHD17B

ABHD17B full-length structure was obtained either from Deepmind Alphafold Structure Database[56] or prepared *de novo* through I-Tasser [57,58]. All models of ABHD17B full-length structure were performed with Maestro and minimized using Schrodinger Protein Preparation Wizard[58,59]. Minimized structures were exported in .pdb format and prepared using solution builder from CHARMM-GUI[60]. Simulations of ABHD17B from I-Tasser and AlphaFold were run to 100 ns, and analysis was performed using VMD and Schrodinger Maestro[58,61]. Molecular dynamics simulations were performed using NAMD 2.12[62] with the CHARMM36m force field[63] on full-length mouse ABHD17B generated from either i-Tasser[64] or AlphaFold2[29]. Systems were prepared using the CHARMM-GUI solution builder with a salt concentration of 150 mM NaCl. Visualization and analyses were performed using VMD 1.9.3[61]. The system was equilibrated for 10 ns restraining the Cα atoms of the protein (1.0 kcal/mol/A2) to allow for solvation. Root mean square deviations (RMSD) using backbone Cα atoms were calculated using VMD RMSD trajectory tool and exported and plotted using Graphpad Prism version 9.

RNA-Seq

HSCs from donor 3 were transfected with NTC si5, *ABHD17B* si1, and *ABHD17B* si4 in triplicate. Cells were harvested in Trizol reagent, and RNA was purified through Direct-zol RNA Miniprep Kit (Cat. # R2050). All samples had RIN scores greater than 9 (Agilent 4150 TapeStation System, G2992 AA) and underwent polyA-selection and stranded library preparation prior to sequencing at 150 paired end reads (Genewiz from Azenta Life Sciences). RNA-seq counts were generated by bcbio-nextgen using salmon[65]. Counts were imported into R using tximport[66] and DESeq2[67]. Gene annotations for pseudo-alignment were obtained from Ensembl, version Homo_sapiens.GRCh38.98. AnnotationHub was used to obtain annotations for the Rscripts. Data

manipulation and plots were performed using Tidyverse[68]. Differential expression analysis was performed using DESeq2[67] with lfcShrinkage using apeglm[69]. Genes were defined as repressed if they were significantly differentially expressed at an adjusted p-value <0.05 for both si1 and si4 compared to control, results for both siRNAs showed a log 2 fold change of less than 0, and at least one siRNA showing log2 fold change less than -0.585 (2/3 reduction in gene expression).

Heatmaps were generated by pheatmap[70]. PCA plots were generated using custom code. clusterProfiler[71] with GOSemSim[72,73] and DOSE[74] were used for functional analysis.

Lentiviral Transduction of HSCs

Lentivirus was produced in HEK-293T cells by transfecting plamids expressing either EGFP_FLAG, ABHD17B-FLAG, or S170A-ABHD17B-FLAG along with pMD2.G (Addgene plasmid # 12259) and psPAX2 (Addgene plasmid # 12260) using X-tremeGENE 9 transfection reagent[22]. Lentivurs was administered with 10 μg/mL polybrene (Sigma-Aldrich, Cat. # TR-1003-G) for 24 hr before the first media change. After 24 hr, cells were selected with puromycin (1 μg/mL, Cat. # A1113803) for 4 days. RNA was harvested in Trizol, and cell lysates for Western blot were harvested in 1μg/ml Pierce IP Lysis buffer.

Precipitation and mass spectrometry.

Precipitation experiments were performed following transduction of HSCs with lentivirus expressing ABHD17B-FLAG or GFP-FLAG. Cells were selected with puromycin (1 μg/ml) for 4 days and grown to confluence before harvest in Pierce Lysis Buffer. Lysates were frozen at -80° C, thawed at 4° C, and cleared by centrifugation at 4500 *g* for 10 min at 4° C. Lysates were

incubated with anti-FLAG (M2) beads on a rocker for 30 min at 4° C with vortexing at 10 min intervals. Beads were washed two times with 1 mL Pierce Lysis Buffer using a magnetic rack and eluted in 100 μl Pierce lysis buffer containing 3X FLAG® Peptide (Sigma, Cat. # F4799) at 20 μM. Eluted proteins were boiled at 95° C, and gel electrophoresis was performed. After electrophoresis, proteins were visualized with Coomassie Blue. Bands were excised above and below the location of GFP protein for MS analysis at the Taplin Mass Spectometry following approaches previously described[75]. Data from two biological experiments, each in duplicate were analyzed. DESeq2[67] was applied to spectral counts to obtain a list of proteins showing differential abundance between ABDH17B IP samples and control GFP IP samples.

Hepatic hydroxyproline

To quantify collagen level, mouse liver samples were isolation from the same region of left liver lobe[76]. Isolated samples were homogenized and processed to evaluate hydroxyproline concentration using hydroxyproline assay kits (Sigma-Aldrich, Cat. # MAK008) following manufacturer's instruction.

Collagen proportionate area (CPA)

CPA was measured as described previously[77]. Livers were fixed in 4% paraformaldehyde at 4° C. After dehydration through graded ethanol and paraffin embedment, samples were sectioned at 5 μm. Pico-Sirius red staining was performed using the left liver lobe from formalin fixed paraffin embedded sections (iHisto). Whole sections were scanned and loaded into ImageJ to calculate the ratio of collagen positive area against the total parenchyma area and expressed as a percentage.

Data Availability

Sequencing data have been deposited in GEO (GSE240123), which will be released upon publication. The following datasets were also used in this study: GSE78853 and GSE68108.

Abbreviations

Ala, alanine; ABHD17B, abhydrolase domain containing 17B; ACTA2 (gene symbol) or aSMA (protein symbol), alpha smooth muscle actin; CCl_4, carbon tetrachloride; COL1A1, collagen type I alpha 1 chain; ECM, extracellular matrix; mRNA, messenger RNA; FDR, false discovery rate; GEO, Gene Expression Omnibus; GFP, green fluorescent protein; GO, gene ontology; HSC, hepatic stellate cell; siRNA, small interfering RNA; ICCB, Institute of Chemistry and Cell Biology; IQR, interquartile range; MS, mass spectrometry; μM, micro molar; NAFLD, non-alcoholic fatty liver disease; ns, nanosecond; NTC, non-targeting control; PSC, primary sclerosing cholangitis; qRT-PCR, quantitative real time polymerase chain reaction; RMSD, root mean square deviation; RNA-seq, RNA sequencing; RT, room temperature; S170A, serine (residue 170 of ABHD17B) to alanine mutation; SEM, standard error of the mean; ser, serine; TGF-β, Transforming growth factor beta; TPM, transcripts per million mapped reads; WT, wildtype.

Acknowledgements

We thank the staff at the ICCB-Longwood Screening Facility, and especially Richard Siu for their assistance in establishing and performing the siRNA screen. We also thank Nicola Zimmermann and Sabine Weigle at Boehringer Ingelheim for conducting the in vitro analysis of α-SMA fibers

and extracellular collagen deposition. We thank members of the Mullen lab and colleagues at Boehringer Ingelheim, including John Broadwater, Peter Seither, and Christofer Tautermann for helpful discussion. We also thank the Taplin Mass Spectrometry Core and Ross Tamiano at Harvard Medical School. This work was funded through a grant from Boehringer Ingelheim Pharma GmbH Co KG. The graphic abstract contains vector images from Servier Medical Art (https://smart.servier.com/) and stock images from BioRender (https://biorender.com).

Competing Interests

A.C.M. receives research funding from GSK for unrelated projects.

Contributions

W.L. and A.C.M. conceived the study with C.B.K., J.F.R., J.F.D, and D.M.S. W.L., R.P.S., and C.S. performed the experiments with assistance from J.Y.C., J.S., S.P.M., M. S., Y.Y., and J.F.D. D.W. supported processing of imaging data. Protein structural analysis was performed by R.P.S. with support from G. A., who also oversaw synthesis and analysis of ABD957. All other computational analyses were performed by L.P., R.K., and V.B.B. under the direction of S.J.H.S. The manuscript was written by W.L., R.P.S., C.S., D.M.S, and A.C.M. with input from all other authors.

References:

[1] Falize L, Guillygomarc'h A, Perrin M, Lainé F, Guyader D, Brissot P, et al. Reversibility of hepatic fibrosis in treated genetic hemochromatosis: A study of 36 cases. Hepatology 2006;44:472–7. https://doi.org/10.1002/hep.21260.

[2] Bonis PAL, Friedman SL, Kaplan MM. Is Liver Fibrosis Reversible? New Engl J Medicine 2001;344:452–4. https://doi.org/10.1056/nejm200102083440610.

[3] Musso G, Gambino R, Cassader M, Pagano G. A meta‐analysis of randomized trials for the treatment of nonalcoholic fatty liver disease. Hepatology 2010;52:79–104. https://doi.org/10.1002/hep.23623.

[4] Sanyal AJ, Chalasani N, Kowdley KV, McCullough A, Diehl AM, Bass NM, et al. Pioglitazone, vitamin E, or placebo for nonalcoholic steatohepatitis. New Engl J Medicine 2010;362:1675–85. https://doi.org/10.1056/nejmoa0907929.

[5] Rinella ME, Lazarus JV, Ratziu V, Francque SM, Sanyal AJ, Kanwal F, et al. A multi-society Delphi consensus statement on new fatty liver disease nomenclature. Hepatology 2023;Publish Ahead of Print. https://doi.org/10.1097/hep.0000000000000520.

[6] Karlsen TH, Folseraas T, Thorburn D, Vesterhus M. Primary sclerosing cholangitis â€" a comprehensive review. Journal of Hepatology 2017;67:1298–323. https://doi.org/10.1016/j.jhep.2017.07.022.

[7] Younossi ZM, Koenig AB, Abdelatif D, Fazel Y, Henry L, Wymer M. Global epidemiology of nonalcoholic fatty liver disease-Meta-analytic assessment of prevalence, incidence, and outcomes. Hepatology 2016;64:73–84. https://doi.org/10.1002/hep.28431.

[8] Younossi ZM, Stepanova M, Ong J, Trimble G, AlQahtani S, Younossi I, et al. Nonalcoholic Steatohepatitis Is the Most Rapidly Increasing Indication for Liver Transplantation in the United States. Clin Gastroenterol H 2021;19:580-589.e5. https://doi.org/10.1016/j.cgh.2020.05.064.

[9] Friedman SL, Roll FJ, Boyles J, Bissell DM. Hepatic lipocytes: the principal collagen-producing cells of normal rat liver. Proceedings of the National Academy of Sciences 1985;82:8681–5.

[10] Maher JJ, McGuire RF. Extracellular matrix gene expression increases preferentially in rat lipocytes and sinusoidal endothelial cells during hepatic fibrosis in vivo. Journal of Clinical Investigation 1990;86:1641–8. https://doi.org/10.1172/jci114886.

[11] Mederacke I, Hsu CC, Troeger JS, Huebener P, Mu X, Dapito DH, et al. Fate tracing reveals hepatic stellate cells as dominant contributors to liver fibrosis independent of its aetiology. Nature Communications 2013;4:1–11. https://doi.org/10.1038/ncomms3823.

[12] Friedman SL. Hepatic Stellate Cells: Protean, Multifunctional, and Enigmatic Cells of the Liver 2008;88:125–72. https://doi.org/10.1152/physrev.00013.2007.

[13] Geerts A. History, Heterogeneity, Developmental Biology, and Functions of Quiescent Hepatic Stellate Cells. Seminars Liver Dis 2001;21:311–36. https://doi.org/10.1055/s-2001-17550.

[14] Bataller R, Brenner DA. Liver fibrosis. Journal of Clinical Investigation 2005;115:209–18. https://doi.org/10.1172/jci200524282.

[15] Kisseleva T, Cong M, Paik Y, Scholten D, Jiang C, Benner C, et al. Myofibroblasts revert to an inactive phenotype during regression of liver fibrosis. Proceedings of the National Academy of Sciences 2012;109:9448–53. https://doi.org/10.1073/pnas.1201840109.

[16] Troeger JS, Mederacke I, Gwak GY, Dapito DH, Mu X, Hsu CC, et al. Deactivation of Hepatic Stellate Cells During Liver Fibrosis Resolution in Mice. Gastroenterology 2012;143:1073-1083.e22. https://doi.org/10.1053/j.gastro.2012.06.036.

[17] Friedman SL, Rockey DC, McGuire RF, Maher JJ, Boyles JK, Yamasaki G. Isolated hepatic lipocytes and Kupffer cells from normal human liver: morphological and functional characteristics in primary culture. Hepatology 1992;15:234–43.

[18] Perea L, Coll M, Sancho-Bru P. Assessment of Liver Fibrotic Insults In Vitro. Methods Mol Biology Clifton N J 2015;1250:391–401. https://doi.org/10.1007/978-1-4939-2074-7_30.

[19] Kisseleva T, Brenner D. Molecular and cellular mechanisms of liver fibrosis and its regression. Nat Rev Gastroentero 2021;18:151–66. https://doi.org/10.1038/s41575-020-00372-7.

[20] Zisser A, Ipsen DH, Tveden-Nyborg P. Hepatic Stellate Cell Activation and Inactivation in NASH-Fibrosis—Roles as Putative Treatment Targets? Biomed 2021;9:365. https://doi.org/10.3390/biomedicines9040365.

[21] Chen JY, Newcomb B, Zhou C, Pondick JV, Ghoshal S, York SR, et al. Tricyclic Antidepressants Promote Ceramide Accumulation to Regulate Collagen Production in Human Hepatic Stellate Cells. Scientific Reports 2017;7:44867–13. https://doi.org/10.1038/srep44867.

[22] Li W, Chen JY, Sun C, Sparks RP, Pantano L, Rahman R-U, et al. Nanchangmycin regulates FYN, PTK2, and MAPK1/3 to control the fibrotic activity of human hepatic stellate cells. Elife 2022;11:e74513. https://doi.org/10.7554/elife.74513.

[23] Johnston SM, Shamu CE, Smith JA. Automation Considerations for RNAi Library Formatting and High Throughput Transfection. eBook. eISBN 978-1-60805-940-9. Frontiers in RNAi 2014;1:21–39.

[24] Zhou C, York SR, Chen JY, Pondick JV, Motola DL, Chung RT, et al. Long noncoding RNAs expressed in human hepatic stellate cells form networks with extracellular matrix proteins. Genome Medicine 2016:1–20. https://doi.org/10.1186/s13073-016-0285-0.

[25] Lin DTS, Conibear E. ABHD17 proteins are novel protein depalmitoylases that regulate N-Ras palmitate turnover and subcellular localization. ELife 2015;4:e11306. https://doi.org/10.7554/elife.11306.

[26] Glass DS, Grossfeld D, Renna HA, Agarwala P, Spiegler P, DeLeon J, et al. Idiopathic pulmonary fibrosis: Current and future treatment. Clin Respir J 2022;16:84–96. https://doi.org/10.1111/crj.13466.

[27] KATZENSTEIN A-LA, MYERS JL. Idiopathic Pulmonary Fibrosis. Am J Resp Crit Care 1998;157:1301–15. https://doi.org/10.1164/ajrccm.157.4.9707039.

[28] Ramos C, Montaño M, García-Alvarez J, Ruiz V, Uhal BD, Selman M, et al. Fibroblasts from Idiopathic Pulmonary Fibrosis and Normal Lungs Differ in Growth Rate, Apoptosis, and Tissue Inhibitor of Metalloproteinases Expression. Am J Resp Cell Mol 2001;24:591–8. https://doi.org/10.1165/ajrcmb.24.5.4333.

[29] Jumper J, Evans R, Pritzel A, Green T, Figurnov M, Ronneberger O, et al. Highly accurate protein structure prediction with AlphaFold. Nature 2021;596:583–9. https://doi.org/10.1038/s41586-021-03819-2.

[30] Rauwerdink A, Kazlauskas RJ. How the Same Core Catalytic Machinery Catalyzes 17 Different Reactions: the Serine-Histidine-Aspartate Catalytic Triad of α/β-Hydrolase Fold Enzymes. Acs Catal 2015;5:6153–76. https://doi.org/10.1021/acscatal.5b01539.

[31] Remsberg JR, Suciu RM, Zambetti NA, Hanigan TW, Firestone AJ, Inguva A, et al. ABHD17 regulation of plasma membrane palmitoylation and N-Ras-dependent cancer growth. Nat Chem Biol 2021;17:856–64. https://doi.org/10.1038/s41589-021-00785-8.

[32] He Y, Shang Y, Li Y, Wang M, Yu D, Yang Y, et al. An 8-ferroptosis-related genes signature from Bronchoalveolar Lavage Fluid for prognosis in patients with idiopathic pulmonary fibrosis. Bmc Pulm Med 2022;22:15. https://doi.org/10.1186/s12890-021-01799-7.

[33] Hagström H, Nasr P, Ekstedt M, Hammar U, Stål P, Hultcrantz R, et al. Fibrosis stage but not NASH predicts mortality and time to development of severe liver disease in biopsy-proven NAFLD. J Hepatol 2017;67:1265–73. https://doi.org/10.1016/j.jhep.2017.07.027.

[34] Sanyal AJ, Natta MLV, Clark J, Neuschwander-Tetri BA, Diehl A, Dasarathy S, et al. Prospective Study of Outcomes in Adults with Nonalcoholic Fatty Liver Disease. N Engl J Med 2021;385:1559–69. https://doi.org/10.1056/nejmoa2029349.

[35] Jansa P, Mason SW, Hoffmann-Rohrer U, Grummt I. Cloning and functional characterization of PTRF, a novel protein which induces dissociation of paused ternary transcription complexes. Embo J 1998;17:2855–64. https://doi.org/10.1093/emboj/17.10.2855.

[36] Hill MM, Bastiani M, Luetterforst R, Kirkham M, Kirkham A, Nixon SJ, et al. PTRF-Cavin, a Conserved Cytoplasmic Protein Required for Caveola Formation and Function. Cell 2008;132:113–24. https://doi.org/10.1016/j.cell.2007.11.042.

[37] Ilha M, Moraes K da S, Rohden F, Martins LAM, Borojevic R, Lenz G, et al. Exogenous expression of caveolin-1 is sufficient for hepatic stellate cell activation. J Cell Biochem 2019;120:19031–43. https://doi.org/10.1002/jcb.29226.

[38] Expert-Bezançon A, Caer JPL, Marie J. Heterogeneous Nuclear Ribonucleoprotein (hnRNP) K Is a Component of an Intronic Splicing Enhancer Complex That Activates the Splicing of the Alternative Exon 6A from Chicken β-Tropomyosin Pre-mRNA*. J Biol Chem 2002;277:16614–23. https://doi.org/10.1074/jbc.m201083200.

[39] Shnyreva M, Schullery DS, Suzuki H, Higaki Y, Bomsztyk K. Interaction of Two Multifunctional Proteins HETEROGENEOUS NUCLEAR RIBONUCLEOPROTEIN K AND Y-BOX-BINDING PROTEIN*. J Biol Chem 2000;275:15498–503. https://doi.org/10.1074/jbc.275.20.15498.

[40] Chen C-Y, Gherzi R, Andersen JS, Gaietta G, Jürchott K, Royer H-D, et al. Nucleolin and YB-1 are required for JNK-mediated interleukin-2 mRNA stabilization during T-cell activation. Gene Dev 2000;14:1236–48. https://doi.org/10.1101/gad.14.10.1236.

[41] Takimoto M, Tomonaga T, Matunis M, Avigan M, Krutzsch H, Dreyfuss G, et al. Specific binding of heterogeneous ribonucleoprotein particle protein K to the human c-myc promoter, in vitro. J Biol Chem 1993;268:18249–58. https://doi.org/10.1016/s0021-9258(17)46837-2.

[42] Laury-Kleintop LD, Tresini M, Hammond O. Compartmentalization of hnRNP-K during cell cycle progression and its interaction with calponin in the cytoplasm. J Cell Biochem 2005;95:1042–56. https://doi.org/10.1002/jcb.20486.

[43] Laury-Kleintop LD, Tresini M, Hammond O. Sub-cellular Localization of hnRNP-K in Smooth Muscle Cells and its Interaction with Calponin. Microsc Microanal 2004;10:1404–5. https://doi.org/10.1017/s1431927604882333.

[44] Reynaert H. Hepatic stellate cells: role in microcirculation and pathophysiology of portal hypertension. Gut 2002;50:571–81. https://doi.org/10.1136/gut.50.4.571.

[45] Zhang L, Tang F, Terracciano L, Hynx D, Kohler R, Bichet S, et al. NDR Functions as a Physiological YAP1 Kinase in the Intestinal Epithelium. Curr Biol 2015;25:296–305. https://doi.org/10.1016/j.cub.2014.11.054.

[46] Liu J, Kong X, Lee YM, Zhang MK, Guo LY, Lin Y, et al. Stk38 Modulates Rbm24 Protein Stability to Regulate Sarcomere Assembly in Cardiomyocytes. Sci Rep-Uk 2017;7:44870. https://doi.org/10.1038/srep44870.

[47] Mochitate K, Pawelek P, Grinnell F. Stress relaxation of contracted collagen gels: Disruption of actin filament bundles, release of cell surface fibronectin, and down-regulation of DNA and protein synthesis. Exp Cell Res 1991;193:198–207. https://doi.org/10.1016/0014-4827(91)90556-a.

[48] Rombouts K, Knittel T, Machesky L, Braet F, Wielant A, Hellemans K, et al. Actin filament formation, reorganization and migration are impaired in hepatic stellate cells under influence of trichostatin A, a histone deacetylase inhibitor. J Hepatol 2002;37:788–96. https://doi.org/10.1016/s0168-8278(02)00275-1.

[49] Sohara N, Znoyko I, Levy MT, Trojanowska M, Reuben A. Reversal of activation of human myofibroblast-like cells by culture on a basement membrane-like substrate 2002:1–8.

[50] Shi Z, Rockey DC. Upregulation of the actin cytoskeleton via myocardin leads to increased expression of type 1 collagen. Lab Invest 2017;97:1412–26. https://doi.org/10.1038/labinvest.2017.96.

[51] Karvar S, Addo EAA, Suda J, Singh S, Zhu L, Li Z, et al. Moesin, an ERM family member, regulates hepatic fibrosis. Hepatology 2019:hep.31078-37. https://doi.org/10.1002/hep.31078.

[52] Rockey DC, Weymouth N, Shi Z. Smooth Muscle α Actin (Acta2) and Myofibroblast Function during Hepatic Wound Healing. Plos One 2013;8:e77166. https://doi.org/10.1371/journal.pone.0077166.

[53] Yenilmez B, Wetoska N, Kelly M, Echeverria D, Min K, Lifshitz L, et al. An RNAi therapeutic targeting hepatic DGAT2 in a genetically obese mouse model of nonalcoholic steatohepatitis. Mol Ther 2022;30:1329–42. https://doi.org/10.1016/j.ymthe.2021.11.007.

[54] Alsamman S, Christenson SA, Yu A, Ayad NME, Mooring MS, Segal JM, et al. Targeting acid ceramidase inhibits YAP/TAZ signaling to reduce fibrosis in mice. Science Translational Medicine 2020;12:eaay8798. https://doi.org/10.1126/scitranslmed.aay8798.

[55] Weigle S, Martin E, Voegtle A, Wahl B, Schuler M. Primary cell-based phenotypic assays to pharmacologically and genetically study fibrotic diseases in vitro. J Biological Methods 2019;6:e115. https://doi.org/10.14440/jbm.2019.285.

[56] Varadi M, Anyango S, Deshpande M, Nair S, Natassia C, Yordanova G, et al. AlphaFold Protein Structure Database: massively expanding the structural coverage of protein-sequence space with high-accuracy models. Nucleic Acids Res 2021;50:D439–44. https://doi.org/10.1093/nar/gkab1061.

[57] Yang J, Yan R, Roy A, Xu D, Poisson J, Zhang Y. The I-TASSER Suite: protein structure and function prediction. Nat Methods 2015;12:7–8. https://doi.org/10.1038/nmeth.3213.

[58] Maestro, S. ed. (2021). Shrödinger Release 2019-1.

[59] Sastry GM, Adzhigirey M, Day T, Annabhimoju R, Sherman W. Protein and ligand preparation: parameters, protocols, and influence on virtual screening enrichments. J Comput Aid Mol Des 2013;27:221–34. https://doi.org/10.1007/s10822-013-9644-8.

[60] Jo S, Kim T, Iyer VG, Im W. CHARMM-GUI: A web-based graphical user interface for CHARMM. J Comput Chem 2008;29:1859–65. https://doi.org/10.1002/jcc.20945.

[61] Humphrey W, Dalke A, Schulten K. VMD: Visual molecular dynamics. J Mol Graphics 1996;14:33–8. https://doi.org/10.1016/0263-7855(96)00018-5.

[62] Phillips JC, Braun R, Wang W, Gumbart J, Tajkhorshid E, Villa E, et al. Scalable molecular dynamics with NAMD. J Comput Chem 2005;26:1781–802. https://doi.org/10.1002/jcc.20289.

[63] Huang J, Rauscher S, Nawrocki G, Ran T, Feig M, Groot BL de, et al. CHARMM36m: an improved force field for folded and intrinsically disordered proteins. Nat Methods 2017;14:71–3. https://doi.org/10.1038/nmeth.4067.

[64] Zhang Y. I-TASSER server for protein 3D structure prediction. Bmc Bioinformatics 2008;9:40. https://doi.org/10.1186/1471-2105-9-40.

[65] Patro R, Duggal G, Love MI, Irizarry RA, Kingsford C. Salmon provides fast and bias-aware quantification of transcript expression. Nat Methods 2017;14:417–9. https://doi.org/10.1038/nmeth.4197.

[66] Soneson C, Love MI, Robinson MD. Differential analyses for RNA-seq: transcript-level estimates improve gene-level inferences. F1000research 2016;4:1521. https://doi.org/10.12688/f1000research.7563.2.

[67] Love MI, Huber W, Anders S. Moderated estimation of fold change and dispersion for RNA-seq data with DESeq2. Genome Biol 2014;15:550. https://doi.org/10.1186/s13059-014-0550-8.

[68] Wickham H, Averick M, Bryan J, Chang W, McGowan L, François R, et al. Welcome to the Tidyverse. J Open Source Softw 2019;4:1686. https://doi.org/10.21105/joss.01686.

[69] Zhu A, Ibrahim JG, Love MI. Heavy-tailed prior distributions for sequence count data: removing the noise and preserving large differences. Bioinformatics 2019;35:2084–92. https://doi.org/10.1093/bioinformatics/bty895.

[70] Kolde, Heatmaps. Raivo 2015. pheatmap: P. n.d.

[71] Yu G, Wang L-G, Han Y, He Q-Y. clusterProfiler: an R Package for Comparing Biological Themes Among Gene Clusters. Omics J Integr Biology 2012;16:284–7. https://doi.org/10.1089/omi.2011.0118.

[72] Yu G. Gene Ontology Semantic Similarity Analysis Using GOSemSim. Methods Mol Biology Clifton N J 2020;2117:207–15. https://doi.org/10.1007/978-1-0716-0301-7_11.

[73] Yu G, Li F, Qin Y, Bo X, Wu Y, Wang S. GOSemSim: an R package for measuring semantic similarity among GO terms and gene products. Bioinformatics 2010;26:976–8. https://doi.org/10.1093/bioinformatics/btq064.

[74] Yu G, Wang L-G, Yan G-R, He Q-Y. DOSE: an R/Bioconductor package for disease ontology semantic and enrichment analysis. Bioinformatics 2015;31:608–9. https://doi.org/10.1093/bioinformatics/btu684.

[75] Chantranupong L, Saulnier JL, Wang W, Jones DR, Pacold ME, Sabatini BL. Rapid purification and metabolomic profiling of synaptic vesicles from mammalian brain. Elife 2020;9:e59699. https://doi.org/10.7554/elife.59699.

[76] Ikenaga N, Peng Z-W, Vaid KA, Liu SB, Yoshida S, Sverdlov DY, et al. Selective targeting of lysyl oxidase-like 2 (LOXL2) suppresses hepatic fibrosis progression and accelerates its reversal. Gut 2017;66:1697. https://doi.org/10.1136/gutjnl-2016-312473.

[77] Sojoodi M, Erstad DJ, Barrett SC, Salloum S, Zhu S, Qian T, et al. Peroxidasin Deficiency Re-programs Macrophages Toward Pro-fibrolysis Function and Promotes Collagen Resolution

in Liver. Cell Mol Gastroenterology Hepatology 2022;13:1483–509. https://doi.org/10.1016/j.jcmgh.2022.01.015.

[78] Snel B, Lehmann G, Bork P, Huynen MA. STRING: a web-server to retrieve and display the repeatedly occurring neighbourhood of a gene. Nucleic Acids Res 2000;28:3442–4. https://doi.org/10.1093/nar/28.18.3442.

[79] Szklarczyk D, Kirsch R, Koutrouli M, Nastou K, Mehryary F, Hachilif R, et al. The STRING database in 2023: protein–protein association networks and functional enrichment analyses for any sequenced genome of interest. Nucleic Acids Res 2022;51:D638–46. https://doi.org/10.1093/nar/gkac1000.

[80] Harder E, Damm W, Maple J, Wu C, Reboul M, Xiang JY, et al. OPLS3: A Force Field Providing Broad Coverage of Drug-like Small Molecules and Proteins. J Chem Theory Comput 2016;12:281–96. https://doi.org/10.1021/acs.jctc.5b00864.

Table 1. siRNA candidates grouped by priority.

Priority	Gene Symbol	Entrez Gene Name	Location	Type(s)
Priority 1	ABCA6	ATP binding cassette subfamily A member 6	Plasma Membrane	transporter
	ABHD17B	abhydrolase domain containing 17B	Plasma Membrane	peptidase
	ALG10	ALG10, alpha-1,2-glucosyltransferase	Cytoplasm	enzyme
	CHD8	chromodomain helicase DNA binding protein 8	Nucleus	enzyme
	CTRC	chymotrypsin C	Extracellular Space	peptidase
	LMLN	leishmanolysin like peptidase	Plasma Membrane	peptidase
	PSMC4	proteasome 26S subunit, ATPase 4	Nucleus	peptidase
	SLC25A32	solute carrier family 25 member 32	Cytoplasm	transporter
	SUPT6H	SPT6 homolog, histone chaperone	Nucleus	transcription regulator
	TGFBR2	transforming growth factor beta receptor 2	Plasma Membrane	kinase
	YY1	YY1 transcription factor	Nucleus	transcription regulator
Priority 2	BRD4	bromodomain containing 4	Nucleus	kinase
	EIF1B	eukaryotic translation initiation factor 1B	Cytoplasm	translation regulator
	GPX7	glutathione peroxidase 7	Cytoplasm	enzyme
	KLF6	Kruppel like factor 6	Nucleus	transcription regulator
Priority 3	AQP3	aquaporin 3 (Gill blood group)	Plasma Membrane	transporter
	CLPP	caseinolytic mitochondrial matrix peptidase proteolytic subunit	Cytoplasm	peptidase
	FGF2	fibroblast growth factor 2	Extracellular Space	growth factor
	HERC2	HECT and RLD domain containing E3 ubiquitin protein ligase 2	Cytoplasm	enzyme
	MAPKAPK2	mitogen-activated protein kinase-activated protein kinase 2	Nucleus	kinase
	MFHAS1	malignant fibrous histiocytoma amplified sequence 1	Cytoplasm	other
	NEK4	NIMA related kinase 4	Nucleus	kinase
	SLC25A29	solute carrier family 25 member 29	Cytoplasm	transporter

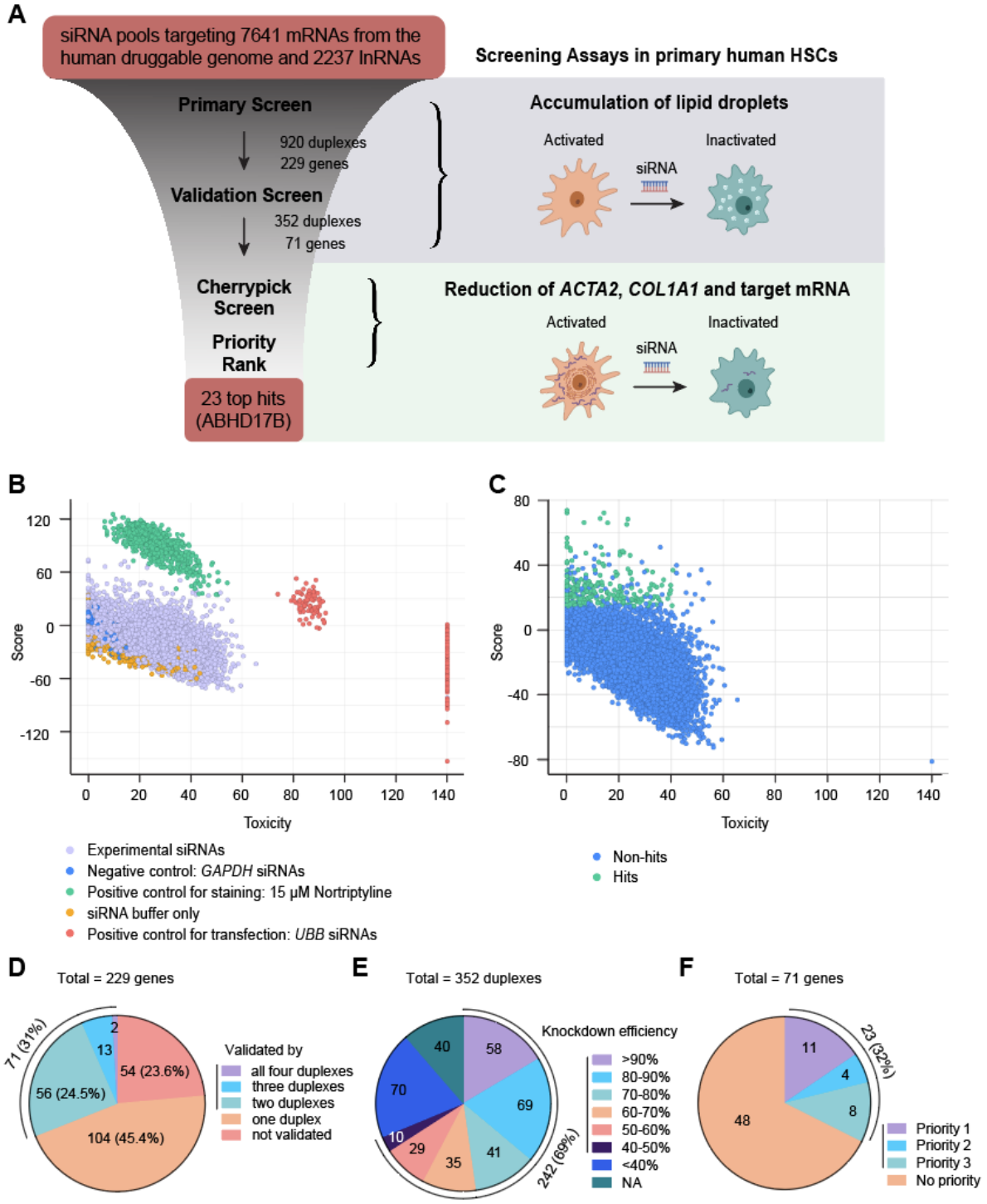
A
siRNA pools targeting 7641 mRNAs from the human druggable genome and 2237 lnRNAs
Screening Assays in primary human HSCs
Primary Screen
920 duplexes
229 genes
Validation Screen
352 duplexes
71 genes
Cherrypick Screen
Priority Rank
23 top hits (ABHD17B)
Accumulation of lipid droplets
Activated
Inactivated
siRNA
Reduction of ACTA2, COL1A1 and target mRNA
Activated
Inactivated
siRNA
B
Score
Toxicity
Experimental siRNAs
Negative control: GAPDH siRNAs
Positive control for staining: 15 µM Nortriptyline
siRNA buffer only
Positive control for transfection: UBB siRNAs
C
Score
Toxicity
Non-hits
Hits
D
Total = 229 genes
71 (31%)
2
13
54 (23.6%)
56 (24.5%)
104 (45.4%)
Validated by
all four duplexes
three duplexes
two duplexes
one duplex
not validated
E
Total = 352 duplexes
40
58
70
69
10
29
35
41
242 (69%)
Knockdown efficiency
>90%
80-90%
70-80%
60-70%
50-60%
40-50%
<40%
NA
F
Total = 71 genes
23 (32%)
11
4
8
48
Priority 1
Priority 2
Priority 3
No priority

Fig. 1. High-throughput screening identified siRNAs that induce HSC myofibroblast inactivation. (A) Overview of the siRNA screen. The assay used in the primary screen and validation screen were based on the accumulation of lipid droplets in inactivated HSCs, while the level of *ACTA2*, *COL1A1,* and the target transcript was measured in the secondary screen. A total of 920 siRNA duplexes targeting 229 genes and a total of 352 siRNA duplexes targeting 71 genes were screened in the validation and cherry pick screen, respectively. (B) Results of the primary siRNA screen. Each dot represents the integrated score and toxicity value of three replicates of an experimental or control well. All wells from the library plates are shown. (C) The score and toxicity values for all experimental wells from the primary screen. (D) Summary of the validation screen results. Approximately 31% of the genes (71 genes) were validated by at least two different siRNA duplexes. (E) Summary of the siRNA knockdown efficiency in the cherry pick screen. For approximately 69% of the siRNA duplexes, the knockdown efficiency was greater than 40%. (F) The ranking of the 71 genes in the cherry pick screen. A total of 23 genes (approximately 32%) were in the high priority group, with 11 (15%) in the Priority 1 group.

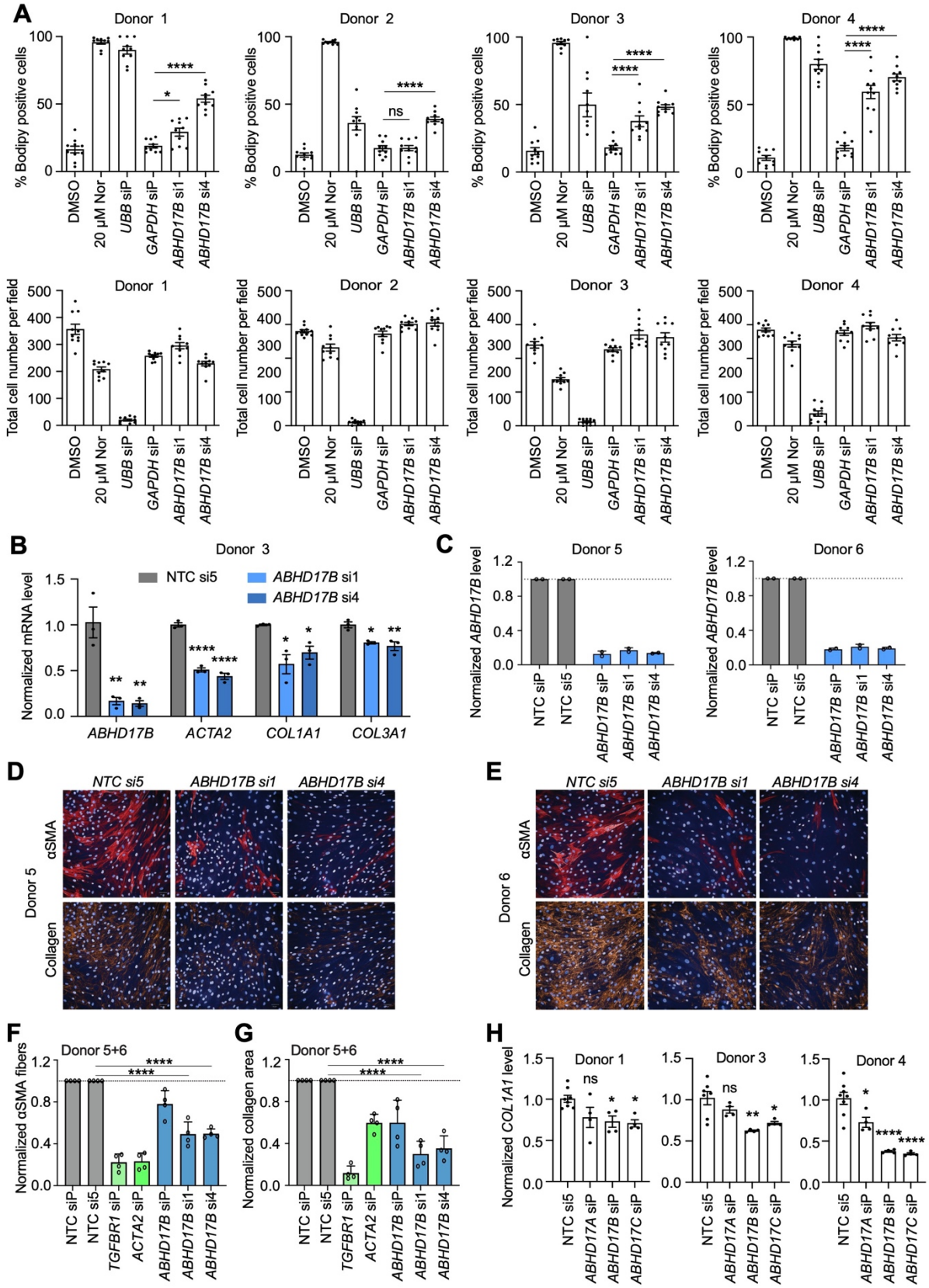
A
Donor 1
Donor 2
Donor 3
Donor 4
% Bodipy positive cells
Total cell number per field
DMSO
20 μM Nor
UBB siP
GAPDH siP
ABHD17B si1
ABHD17B si4
B
Donor 3
NTC si5
ABHD17B si1
ABHD17B si4
Normalized mRNA level
ABHD17B
ACTA2
COL1A1
COL3A1
C
Donor 5
Donor 6
Normalized ABHD17B level
NTC siP
NTC si5
ABHD17B siP
ABHD17B si1
ABHD17B si4
D
NTC si5
ABHD17B si1
ABHD17B si4
αSMA
Collagen
Donor 5
E
Donor 6
F
Donor 5+6
Normalized αSMA fibers
TGFBR1 siP
ACTA2 siP
G
Normalized collagen area
H
Normalized COL1A1 level
ABHD17A siP
ABHD17C siP

Fig. 2. *ABHD17B* knockdown inactivates HSCs and inhibits collagen expression. (A) Effect of *ABHD17B* depletion on lipid accumulation in primary human HSCs from four different donors (top). DMSO and 20 μM nortriptyline (Nor) were used as negative and positive controls for Bodipy staining. The siRNA pool targeting *UBB* served as a control for transfection efficiency, as indicated by the reduction of cell number (bottom). Each dot represents one biological replicate. Error bars represent mean ± SEM (n=10). ns indicates not significant, * indicates $p<0.05$, and **** indicates $p<0.0001$ (one-way ANOVA test). (B) Effect of *ABHD17B* depletion on *ACTA2*, *COL1A1* and *COL3A1* comparing to a non-targeting control (NTC) siRNA 2 days after transfection. Each dot represents one biological replicate. Error bars represent mean ± SEM (n=3). * indicates $p<0.05$, ** indicates $p<0.01$, and **** indicates $p<0.0001$ (one-way ANOVA test). Data are representative of three independent experiments. (C) Primary human HSCs from donors 5 and 6 were transfected with siRNAs as indicated and *ABDH17B* expression was quantified by qRT-PCR 3 days after transfection. Nontargeting control pooled siRNA (NTC siP) and NTC si5 are compared to pooled ABHD17B (siP) siRNAs, *ABHD17B si1*, and *ABHD17B si4*. Error bars represent mean ± SD. (D-E) Scar-in-a-jar assay. HSCs from donor 5 and donor 6 were transfected with single siRNA duplexes: *NTC si5*, *ABDH17B si1,* or *ABDH17B si4*. HSCs were serum starved the day after transfection followed by stimulation with TGF-β in conditions of molecular crowding for 72 hr. α–SMA (red) and collagen (orange) were visualized by immunofluorescence in the same field of view. Nuclei were stained with Hoechst (blue). (F) Quantification of αSMA from scar-in-a-jar assay. Normalized αSMA fiber score is displayed for *NTC siP* and *NTC si5* controls compared to siRNAs targeting *ABHD17B* (*siP*, *si1* and *si4*) and siRNAs targeting *ACTA2* and *TGFRB1* as positive controls. Data from Donors 5 and 6 are combined. Error bars represent mean ± SD. **** indicates $p<0.0001$ comparing nontargeting control (NTC) si5 to *ABHD17B si1* or *ABHD17B si4*. $p<0.0001$ for pooled *TGFBR1* siRNA (*TGFBR siP)* and *siACTA2 siP* compared *to pooled* (*siP*) *NTC,* and $p<0.01$ for *ABHD17B siP* compared to *NTC siP* (Dunnetts multiple comparison test). (G)

Normalized quantification of collagen area is shown for the scar-in-a-jar assay. Conditions are the same as in (F). Error bars represent mean ± SD. **** indicates p<0.0001 comparing nontargeting control (NTC) si5 to *ABHD17B si1* or *ABHD17B si4.* p<0.0001 for pooled *TGFBR1* siRNA (*TGFBR siP)* compared to *NTC siP,* and p <0.01 for *ACTA2 siP* and *ABHD17B siP* compared to *NTC siP* (Dunnetts multiple comparison test). H. Members of the ABHD17 family were depleted using pooled siRNAs in HSCs from human donors 1, 3 and 4. *COL1A1* levels were quantified by qRT-PCR 3 days aftert transfection. Each dot represents one biological replicate. Error bars represent mean ± SEM (n≥4). ns indicates not significant, * indicates p<0.05, ** indicates p<0.01, and **** indicates p<0.0001 (one-way ANOVA test).

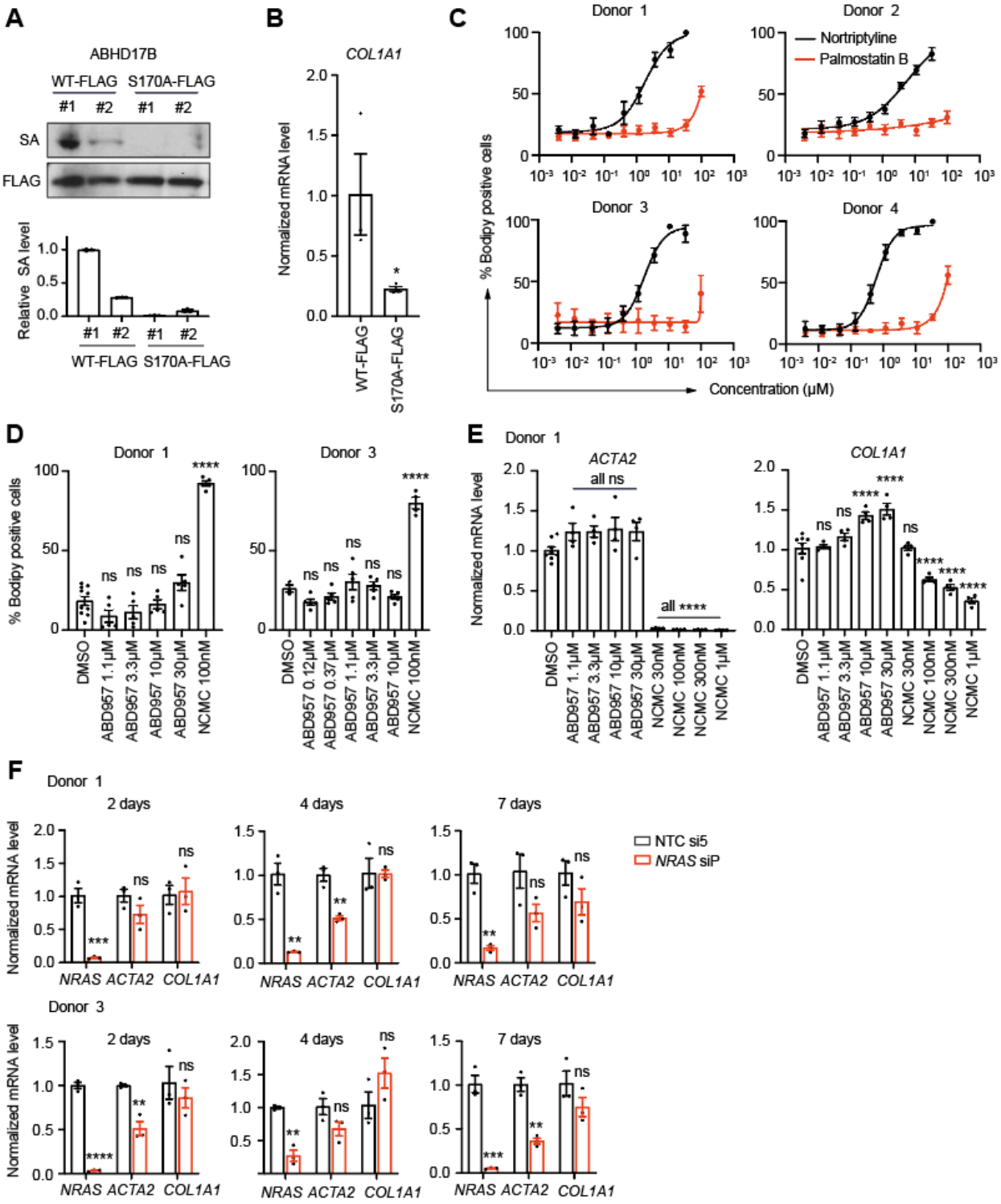
A
ABHD17B
WT-FLAG S170A-FLAG
#1 #2 #1 #2
SA
FLAG
Relative SA level
WT-FLAG S170A-FLAG
B
COL1A1
Normalized mRNA level
WT-FLAG
S170A-FLAG
C
Donor 1
Donor 2
Donor 3
Donor 4
Nortriptyline
Palmostatin B
% Bodipy positive cells
Concentration (μM)
D
Donor 1
Donor 3
% Bodipy positive cells
DMSO
ABD957 1.1μM
ABD957 3.3μM
ABD957 10μM
ABD957 30μM
NCMC 100nM
ABD957 0.12μM
ABD957 0.37μM
E
Donor 1
ACTA2
COL1A1
all ns
all ****
Normalized mRNA level
NCMC 30nM
NCMC 300nM
NCMC 1μM
F
Donor 1
Donor 3
2 days
4 days
7 days
NTC si5
NRAS siP
NRAS ACTA2 COL1A1

Fig. 3. The depalmitoylating activity of ABHD17B and depalmitoylation target NRAS are not required for HSC inactivation or collagen expression. (A) HEK-293T cells were transfected with plasmids expressing wildtype (WT) ABHD17B-FLAG and ABHD17B-S170A-FLAG. Cells were lysed and then treated with a desthiobiotin-labeled serine based activity probe (SABP) on M2 anti-FLAG beads. Serine activity was quantified by streptavidin HRP, and protein levels bound to M2 beads were quantified by probing with anti-FLAG antibody. ABHD17B-FLAG (n=2) and ABHD17B-S170A-FLAG (n=2) were probed for streptavidin (SA) to detect SABP activity and FLAG as a loading control. Top: representative Western blot images, Bottom: quantification of the Western blot images. Each band was quantified three times using Fiji. Error bars represent mean ± SEM. Results are representative of two independent experiments. (B) Expression of *COL1A1* as quantified by qRT-PCR in HSCs transduced with lentivirus expressing WT ABHD17B-FLAG or ABHD17B-S170A-FLAG. Expression was normalized to *PSMB2* as an endogenous control. Error bars represent mean ± SEM (n=3). * indicates $p<0.05$ (t-test). This experiment is representative of two independent experiments. (C) HSCs from four different human donors were treated with nortriptyline or palmostatin B at concentrations as indicated for 48 hr. Cells were then fixed and stained with Bodipy and Hoechst. Each dot represents the averaged value of six replicates. Error bars represent mean ± SD (n=6). (D) HSCs from two different human donors were treated with ABD957 at indicated concentrations at 48 hr. Nanchangmycin (NCMC) served as a positive control[21]. Cells were then fixed and stained with Bodipy and Hoechst. Each dot represents one biological replicate. Error bars represent mean ± SEM (n≥5). ns indicates not significant and **** indicates $p<0.0001$ (one-way ANOVA test). (E) HSCs from human donors 1 and 3 were treated with ABD957 or nanchangmycin (NCMC) at concentrations as indicated for 48 hr. Cells were then lysed for RNA extraction and qRT-PCR analysis of *ACTA2* (left) and *COL1A1* (right). Each dot represents one biological replicate. Error bars represent mean ± SEM (n≥4). ns indicates not significant and **** indicates $p<0.0001$ (one-way ANOVA test). (F) HSCs from human donors 1 and 3 were transfected with non-targeting control siRNA (NTC si5) or pooled

siRNAs targeting *NRAS* (*NRAS* siP), and cells were lysed for qRT-PCR analysis of *NRAS*, *ACTA2,* and *COL1A1* at days 2, 4 and 7 after transfection. Each dot represents one biological replicate. Error bars represent mean ± SEM (n=3). ns indicates not significant, ** indicates $p<0.01$, *** indicates $p<0.001$, and **** indicates $p<0.0001$ (one-way ANOVA test).

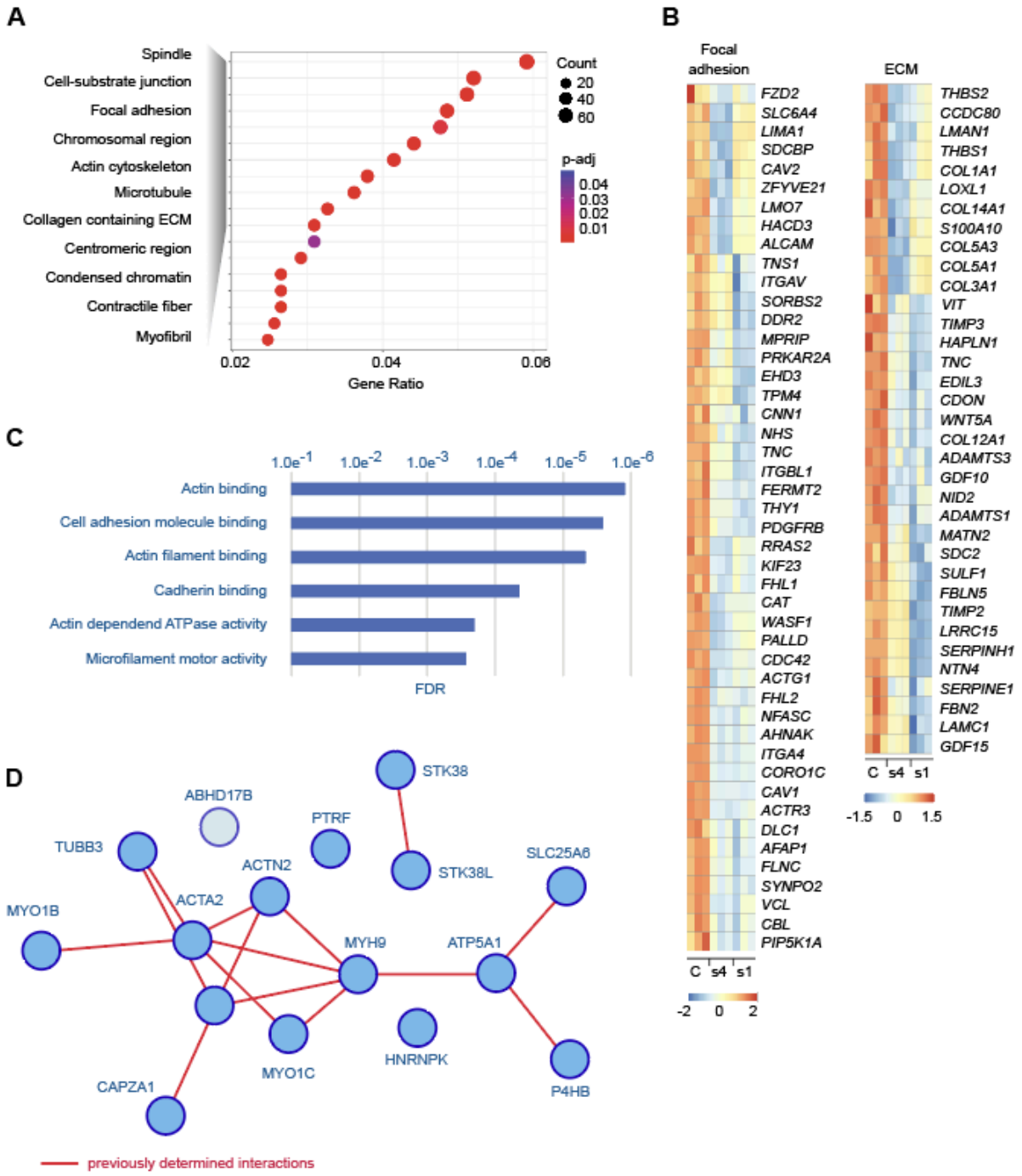
A
Spindle
Cell-substrate junction
Focal adhesion
Chromosomal region
Actin cytoskeleton
Microtubule
Collagen containing ECM
Centromeric region
Condensed chromatin
Contractile fiber
Myofibril
0.02
0.04
0.06
Gene Ratio
Count
20
40
60
p-adj
0.04
0.03
0.02
0.01
B
Focal adhesion
FZD2
SLC6A4
LIMA1
SDCBP
CAV2
ZFYVE21
LMO7
HACD3
ALCAM
TNS1
ITGAV
SORBS2
DDR2
MPRIP
PRKAR2A
EHD3
TPM4
CNN1
NHS
TNC
ITGBL1
FERMT2
THY1
PDGFRB
RRAS2
KIF23
FHL1
CAT
WASF1
PALLD
CDC42
ACTG1
FHL2
NFASC
AHNAK
ITGA4
CORO1C
CAV1
ACTR3
DLC1
AFAP1
FLNC
SYNPO2
VCL
CBL
PIP5K1A
C s4 s1
-2 0 2
ECM
THBS2
CCDC80
LMAN1
THBS1
COL1A1
LOXL1
COL14A1
S100A10
COL5A3
COL5A1
COL3A1
VIT
TIMP3
HAPLN1
TNC
EDIL3
CDON
WNT5A
COL12A1
ADAMTS3
GDF10
NID2
ADAMTS1
MATN2
SDC2
SULF1
FBLN5
TIMP2
LRRC15
SERPINH1
NTN4
SERPINE1
FBN2
LAMC1
GDF15
C s4 s1
-1.5 0 1.5
C
1.0e-1
1.0e-2
1.0e-3
1.0e-4
1.0e-5
1.0e-6
Actin binding
Cell adhesion molecule binding
Actin filament binding
Cadherin binding
Actin dependend ATPase activity
Microfilament motor activity
FDR
D
STK38
ABHD17B
PTRF
TUBB3
STK38L
SLC25A6
ACTN2
ACTA2
MYO1B
MYH9
ATP5A1
MYO1C
HNRNPK
CAPZA1
P4HB
previously determined interactions

Fig. 4. ABDH17B interacts with pathways involving the cytoskeleton, contractility, cell adhesion and ECM. (A) RNA sequencing and differential expression analysis were performed using nontargeting control (NTC) si5, and two siRNAs (siRNA#1 and #4) targeting *ABHD17B*. Dot plot displays the Gene Ontology (GO) terms most enriched in the repressed gene set as a result of ABHD17B depletion. The color of each dot represents the adjusted p value, and the size of the dot represents gene count. (B) Heatmaps show expression of the repressed gene set for indicated GO categories for HSCs transfected with NTC (C), siRNA #4 targeting *ABHD17B* (s4) and siRNA #1 targeting *ABHD17B (*s1*).* Expression is centered and scaled by row (gene). (C) Proteins that interact with ABHD17B were identified by precipitation of ABHD17B-FLAG followed by mass spectrometry (MS) (**Supplementary Table 7**). Enrichment of GO categories (Molecular Functions) for the 15 proteins showing the strongest interaction with ABHD17B (String-db.org)[78,79] is shown. (D) The interactions between the 15 proteins showing the strongest interaction with ABHD17B are displayed in addition to ABHD17B. Dark red lines indicate prior experimentally-determined interactions (String-db.org).

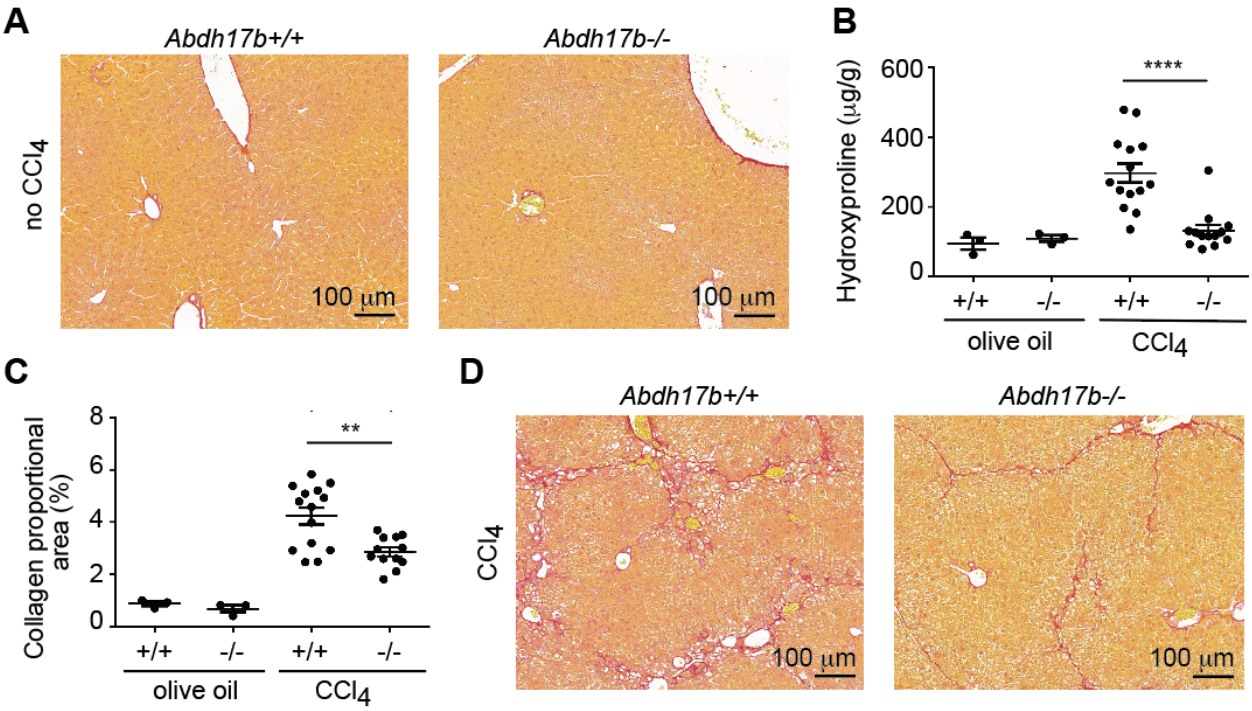
A
Abdh17b+/+
Abdh17b-/-
no CCl4
100 μm
100 μm
B
Hydroxyproline (μg/g)
600
400
200
0
****
+/+
-/-
+/+
-/-
olive oil
CCl4
C
Collagen proportional area (%)
8
6
4
2
0
**
+/+
-/-
+/+
-/-
olive oil
CCl4
D
Abdh17b+/+
Abdh17b-/-
CCl4
100 μm
100 μm

Fig. 5. Loss of *Abhd17b* protects against the development of liver fibrosis. (A) Sirius red staining was performed for *Abhd17*+/+ and *Abhd17*-/- mouse livers in the absence of fibrosis. These mice received control olive oil gavage three times a week for four weeks. (B) Wildtype and *Abhd17b*-/- male mice were treated with carbon tetrachloride (CCl_4) via oral gavage three times a week versus olive oil control gavage. Hydroxyproline analysis was performed after four weeks. Error bars represent mean ± SEM (n=14, 12), **** indicates $p<0.0001$ (t-test). (C) Collagen proportional area (CPA) was calculated for mice under the same conditions as in B, based on Sirius red staining. Error bars represent mean ± SEM (n=14, 12), ** indicates $p<0.01$ (t-test). (D) Representative examples of Sirius red staining for *Abhd17*+/+ and *Abhd17b*-/- mice receiving CCl_4 as in (B).

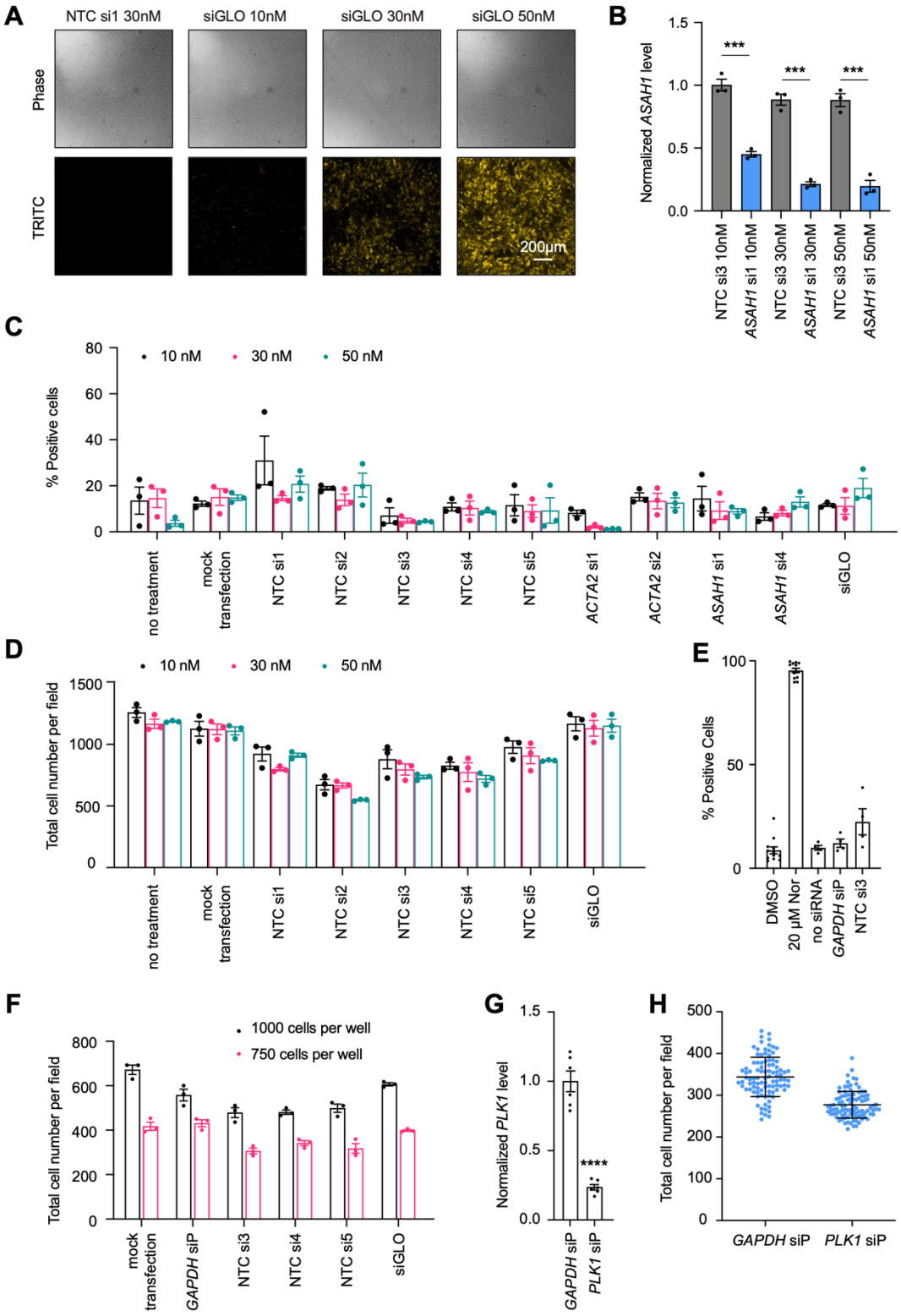
A
NTC si1 30nM
siGLO 10nM
siGLO 30nM
siGLO 50nM
Phase
TRITC
200µm
B
Normalized ASAH1 level
1.5
1.0
0.5
0.0
***
***
***
NTC si3 10nM
ASAH1 si1 10nM
NTC si3 30nM
ASAH1 si1 30nM
NTC si3 50nM
ASAH1 si1 50nM
C
% Positive cells
80
60
40
20
0
10 nM
30 nM
50 nM
no treatment
mock transfection
NTC si1
NTC si2
NTC si3
NTC si4
NTC si5
ACTA2 si1
ACTA2 si2
ASAH1 si1
ASAH1 si4
siGLO
D
Total cell number per field
1500
1000
500
0
10 nM
30 nM
50 nM
no treatment
mock transfection
NTC si1
NTC si2
NTC si3
NTC si4
NTC si5
siGLO
E
% Positive Cells
100
50
0
DMSO
20 µM Nor
no siRNA
GAPDH siP
NTC si3
F
Total cell number per field
800
600
400
200
0
1000 cells per well
750 cells per well
mock transfection
GAPDH siP
NTC si3
NTC si4
NTC si5
siGLO
G
Normalized PLK1 level
1.5
1.0
0.5
0.0
****
GAPDH siP
PLK1 siP
H
Total cell number per field
500
400
300
200
100
0
GAPDH siP
PLK1 siP

Supplementary Fig. 1. Optimization of siRNA transfection protocol in human primary HSCs. (A) Primary HSCs from donor 1 were transfected with non-targeting (NTC) siRNA or siGLO at different concentrations as indicated. Cells were imaged 72hr after transfection. Representative images are shown. Scale bar represents 200 μm. (B) Primary HSCs from donor 1 were transfected with non-targeting siRNA or siRNA targeting *ASAH1*[21] at different concentrations as indicated, and cells were lysed for RNA extraction at 72 hr after transfection. The knockdown efficiency was determined by qRT-PCR. Each dot represents one biological replicate. Error bars represent mean ± SEM. *** indicates $p<0.001$ (n=3, t test). (C-D) Primary HSCs from donor 1 were transfected with different non-targeting control (NTC) siRNA, siRNA targeting *ACTA2*, *ASAH1*, or siGLO at different concentrations as indicated, and cells were fixed for Hoechst and Bodipy staining 72 hr after transfection. Cells were not treated with transfection reagents nor siRNAs in the "no treatment" group, while cells were treated with transfection reagents without siRNAs in the "mock transfection" group. Each dot represents one biological replicate (n=3). Error bars represent mean ± SEM. C: percentage of Bodipy positive cells. D: total count of nuclei per microscopic imaging field. (E) Primary HSCs from donor 1 were treated with DMSO or nortriptyline for 48 hr (used as controls for Bodipy staining) or transfected with siRNAs as indicated for 72 hr. Cells were then fixed and stained with Bodipy and Hoechst to determine the percentage of Bodipy positive cells. Each dot represents one biological replicate. Error bars represent mean ± SEM. (F) Primary HSCs were seeded at two densities in 384-well plates and transfected with 25 nM siRNAs as indicated, and cells were fixed for Hoechst staining 72 hr after transfection. Each dot represents one biological replicate (n=3). Error bars represent mean ± SEM. (G-H) Primary HSCs were transfected with 25 nM pooled siRNAs targeting *PLK1*, and cells were lysed for RNA extraction (G) or fixed for Hoechst staining (H) 72 hr after transfection. G: The knockdown efficiency was determined by qRT-PCR. Each dot represents one biological replicate. Error bars represent mean ± SEM. **** indicates $p<0.0001$ (n=6, t test). H: The number of cells was determined by nuclei count. Each dot represents one biological replicate (n=96). Error bars represent mean ± SD.

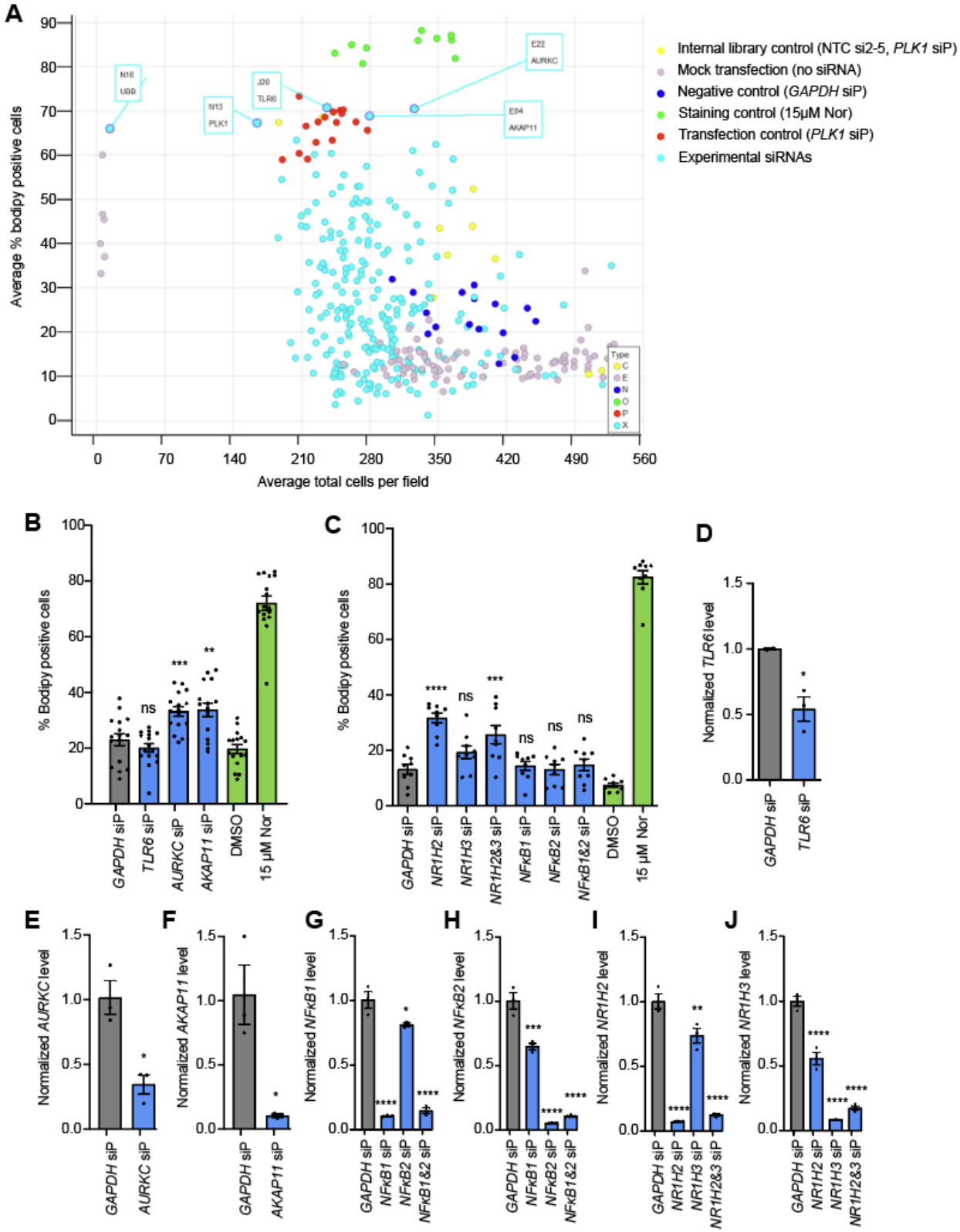
A
Average % bodipy positive cells
Average total cells per field
N16
UBB
N13
PLK1
J20
TLR6
E22
AURKC
E04
AKAP11
Internal library control (NTC si2-5, PLK1 siP)
Mock transfection (no siRNA)
Negative control (GAPDH siP)
Staining control (15μM Nor)
Transfection control (PLK1 siP)
Experimental siRNAs
Type
C
E
N
O
P
X
B
% Bodipy positive cells
GAPDH siP
TLR6 siP
AURKC siP
AKAP11 siP
DMSO
15 μM Nor
C
% Bodipy positive cells
GAPDH siP
NR1H2 siP
NR1H3 siP
NR1H2&3 siP
NFκB1 siP
NFκB2 siP
NFκB1&2 siP
DMSO
15 μM Nor
D
Normalized TLR6 level
GAPDH siP
TLR6 siP
E
Normalized AURKC level
GAPDH siP
AURKC siP
F
Normalized AKAP11 level
GAPDH siP
AKAP11 siP
G
Normalized NFκB1 level
GAPDH siP
NFκB1 siP
NFκB2 siP
NFκB1&2 siP
H
Normalized NFκB2 level
GAPDH siP
NFκB1 siP
NFκB2 siP
NFκB1&2 siP
I
Normalized NR1H2 level
GAPDH siP
NR1H2 siP
NR1H3 siP
NR1H2&3 siP
J
Normalized NR1H3 level
GAPDH siP
NR1H2 siP
NR1H3 siP
NR1H2&3 siP

Supplementary Fig. 2. Pilot siRNA library screen and evaluation of potential positive controls. (A) Summary of the pilot siRNA screen results. Each dot represents the average % Bodipy positive cells and average total cells per field of three replicates of an experimental or control well. All wells from the pilot library plate are shown. The experimental siRNAs with high % Bodipy positive cells or low cell numbers are labeled with well ID and target gene symbol. (B-C) HSCs were treated with siRNAs, DMSO, or nortriptyline (Nor) as indicated, and 72 hr later, cells were fixed and stained with Hoechst and Bodipy. Each dot represents one biological replicate. Error bars represent mean ± SEM. ns indicates not significant, ** indicates $p<0.01$, *** indicates $p<0.001$, and **** indicates $p<0.0001$ compared to the negative control *GAPDH* siP (n=16, one-way ANOVA test). (D-J) HSCs were treated with siRNAs, DMSO, or nortriptyline as indicated, and 72 hr later, cells were lysed for RNA extraction. Knockdown efficiency was evaluated by qRT-PCR. Each dot represents one biological replicate. Error bars represent mean ± SEM. * indicates $p<0.05$, ** indicates $p<0.01$, *** indicates $p<0.001$, and **** indicates $p<0.0001$ compared to the negative control *GAPDH* siP (n=3, t test for D-F and one-way ANOVA test for G-J).

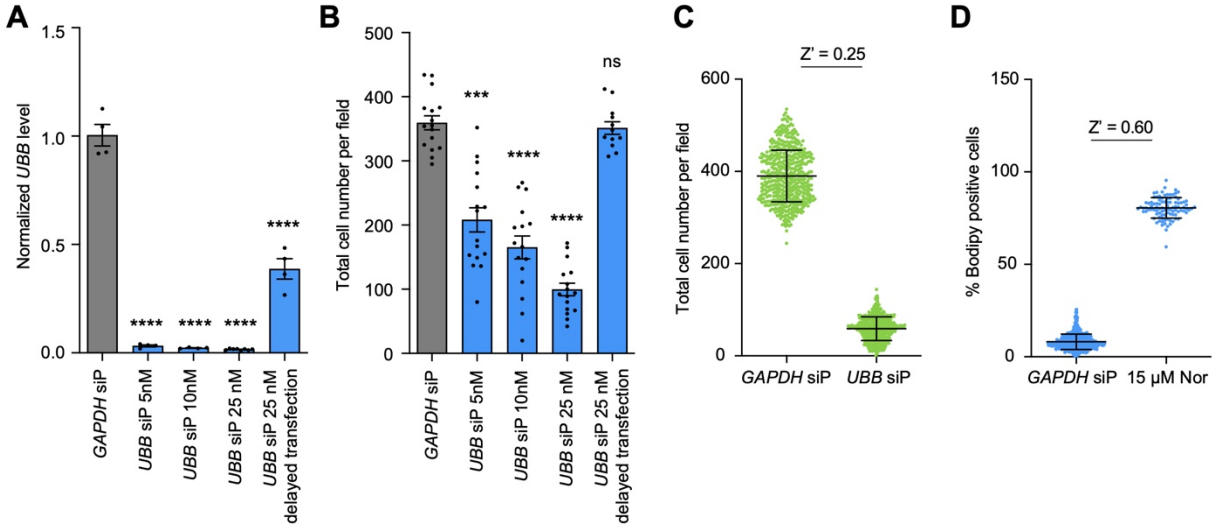

Supplementary Fig. 3. *UBB* siP as an indicator of transfection efficiency. (A-B) Primary human HSCs from donor 1 were transfected with pooled *UBB* siRNAs (siP) at the concentrations indicated. For the "delayed transfection" test condition, transfection reagents were added later than the optimal time frame to confirm that the reagents were not toxic by themselves. Cells were lysed for RNA extraction (A) or fixed and stained with Hoechst (B) 72 hr after transfection. Each dot represents one biological replicate. Error bars represent mean ± SEM. ns indicates not significant, *** indicates $p<0.001$, and **** indicates $p<0.0001$ compared to the negative control *GAPDH* siP ($n\geq4$ as indicated by the number of dots, one-way ANOVA test). A: depletion efficiency was determined by qRT-PCR. B: Total cell number per field was quantified based on nuclei count. (C) Primary human HSCs from donor 1 were transfected with pooled *GAPDH* or *UBB* siRNAs at 25 nM. Cells were fixed and stained with Hoechst 72 hr after transfection to quantify cell number. Each dot represents one biological replicate (n=528). Error bars represent mean ± SD. (D) Primary human HSCs from donor 1 were treated with pooled *GAPDH* siRNAs at 25 nM or nortriptyline (Nor) at 15 μM for 72 hr before cells were fixed and stained with Bodipy and Hoechst. Each dot represents one biological replicate (n=528 for *GAPDH* siP, n=96 for Nor). Error bars represent mean ± SD.

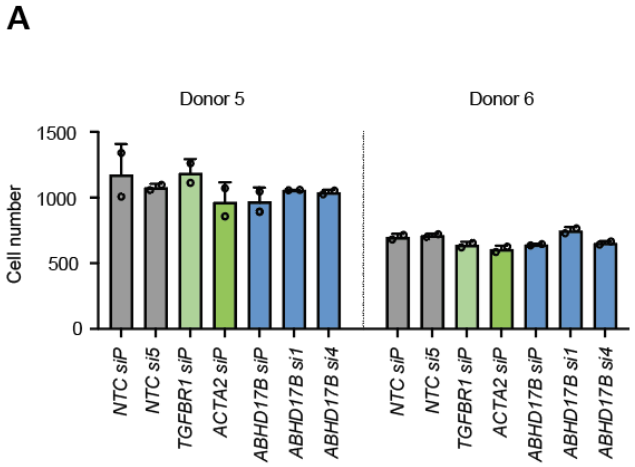
A
Donor 5
Donor 6
Cell number
1500
1000
500
0
NTC siP
NTC si5
TGFBR1 siP
ACTA2 siP
ABHD17B siP
ABHD17B si1
ABHD17B si4
NTC siP
NTC si5
TGFBR1 siP
ACTA2 siP
ABHD17B siP
ABHD17B si1
ABHD17B si4

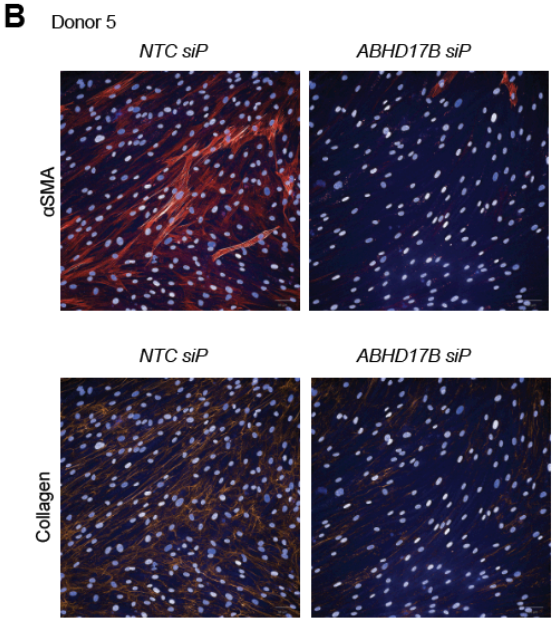
B
Donor 5
NTC siP
ABHD17B siP
αSMA
NTC siP
ABHD17B siP
Collagen

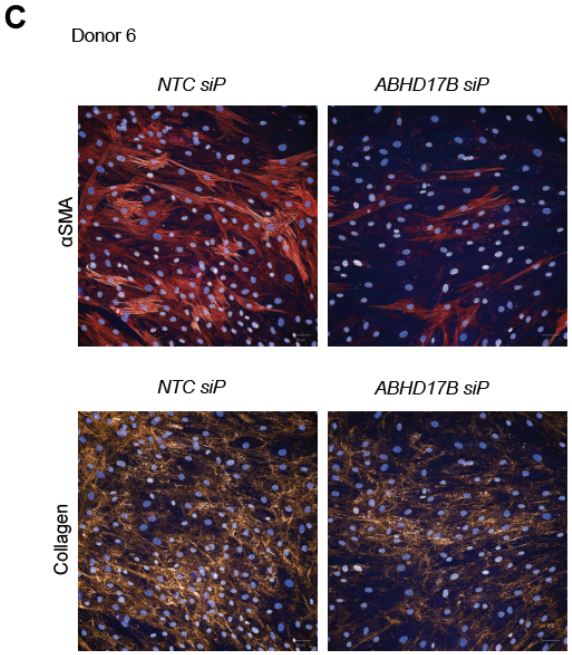
C
Donor 6
NTC siP
ABHD17B siP
αSMA
NTC siP
ABHD17B siP
Collagen

Supplementary Fig. 4. Scar-in-a-jar assay. (A) Primary human HSCs from donors 5 and 6 were transfected with siRNAs as indicated and cell numbers were quantified by nuclei (Hoescht) 3 days after transfection. Nontargeting control pooled siRNA (NTC siP) and NTC si5 are compared to pooled ABHD17B (siP) siRNA, *ABHD17B si1*, *ABHD17B si4*, and control siRNAs targeting *ACTA2* and *TGFBR1*. Error bars represent mean ± SD for two biological replicates (open circles). (B) HSCs from donor 5 were transfected with pooled nontargeting control (*NTC siP*) and pooled siRNAs targeting *ABHD17B* (*ABHD17B siP*). HSCs were serum starved the day after transfection followed by stimulation with TGF-β in conditions of molecular crowding for 72 hr. αSMA (red) and collagen (orange) were visualized by immunofluorescence in the same field. Nuclei were stained with Hoechst (blue). (C) Analysis was performed for donor 6 as in (B).

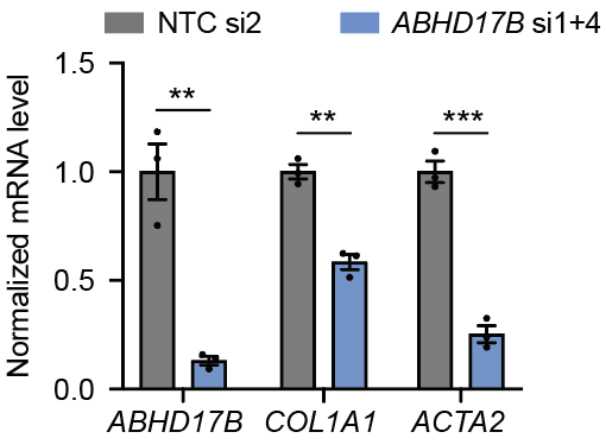

Supplemental Fig. 5. *ABHD17B* regulates *COL1A1* in lung fibroblasts. Primary human lung fibroblasts were transfected with siRNAs, serum starved, and treated with TGFβ. mRNA expression was quantified 72 hr after transfection. Each dot represents one biological replicate. Error bars represent mean ± SEM. ** indicates $p<0.01$, and *** indicates $p<0.001$ (n=3, t test). Data are representative of three independent experiments. NTC si 2 was used as negative control and compared to depletion of *ABDH17B* with si1 and si4.

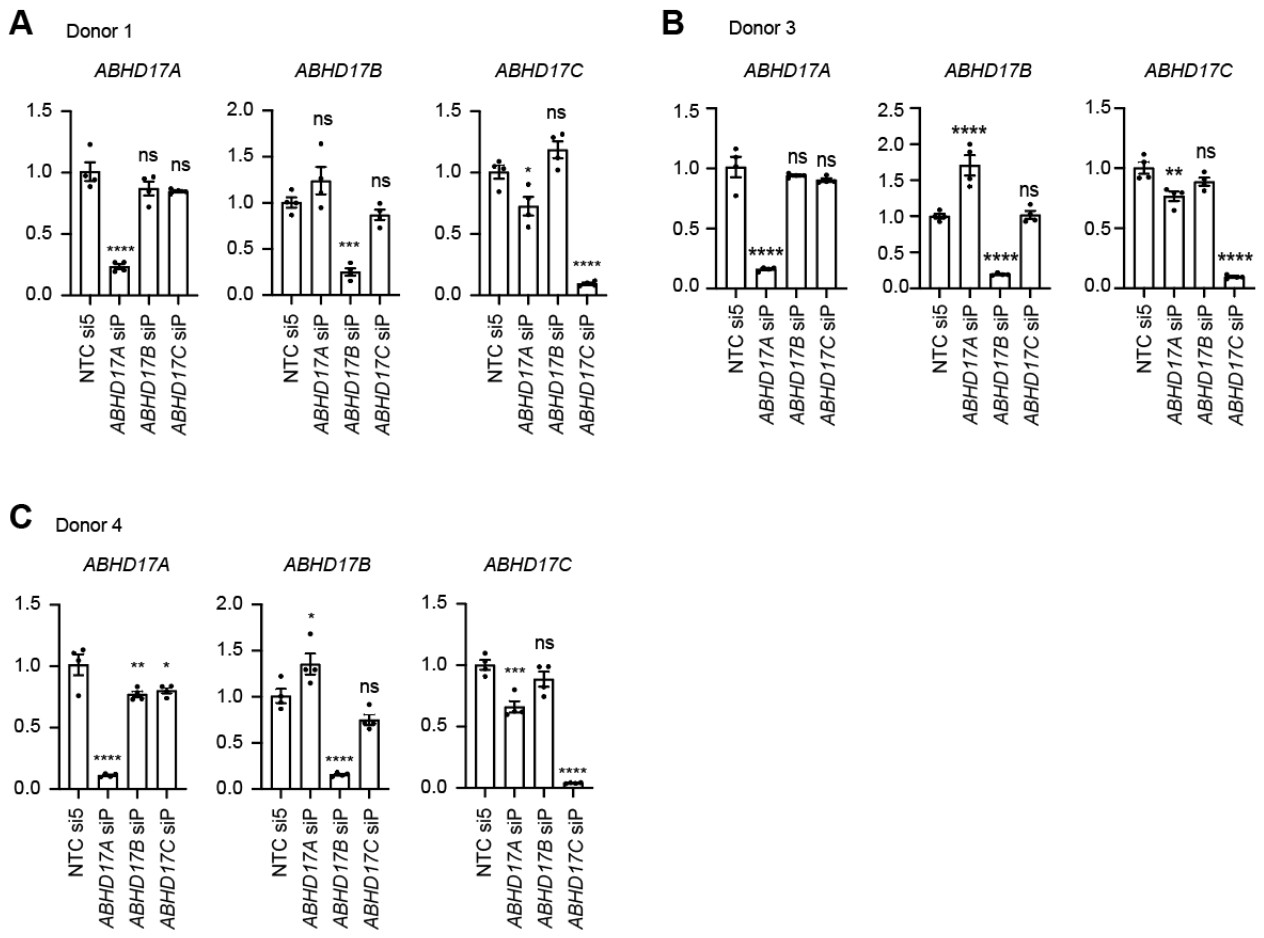

Supplementary Fig. 6. Efficiency of siRNAs targeting each of the ABHD17 family members. Members of the ABHD17 family were depleted using pooled siRNAs in HSCs from human donors 1 (A), 3 (B), and 4 (C). *ABHD17A*, *ABHD17B*, and *ABHD17C* levels 72 hr post transfection were quantified by qRT-PCR. Each dot represents one biological replicate. Error bars represent mean ± SEM (n=4). ns indicates not significant, * indicates $p<0.05$, *** indicates $p<0.001$, and **** indicates $p<0.0001$ (one-way ANOVA test).

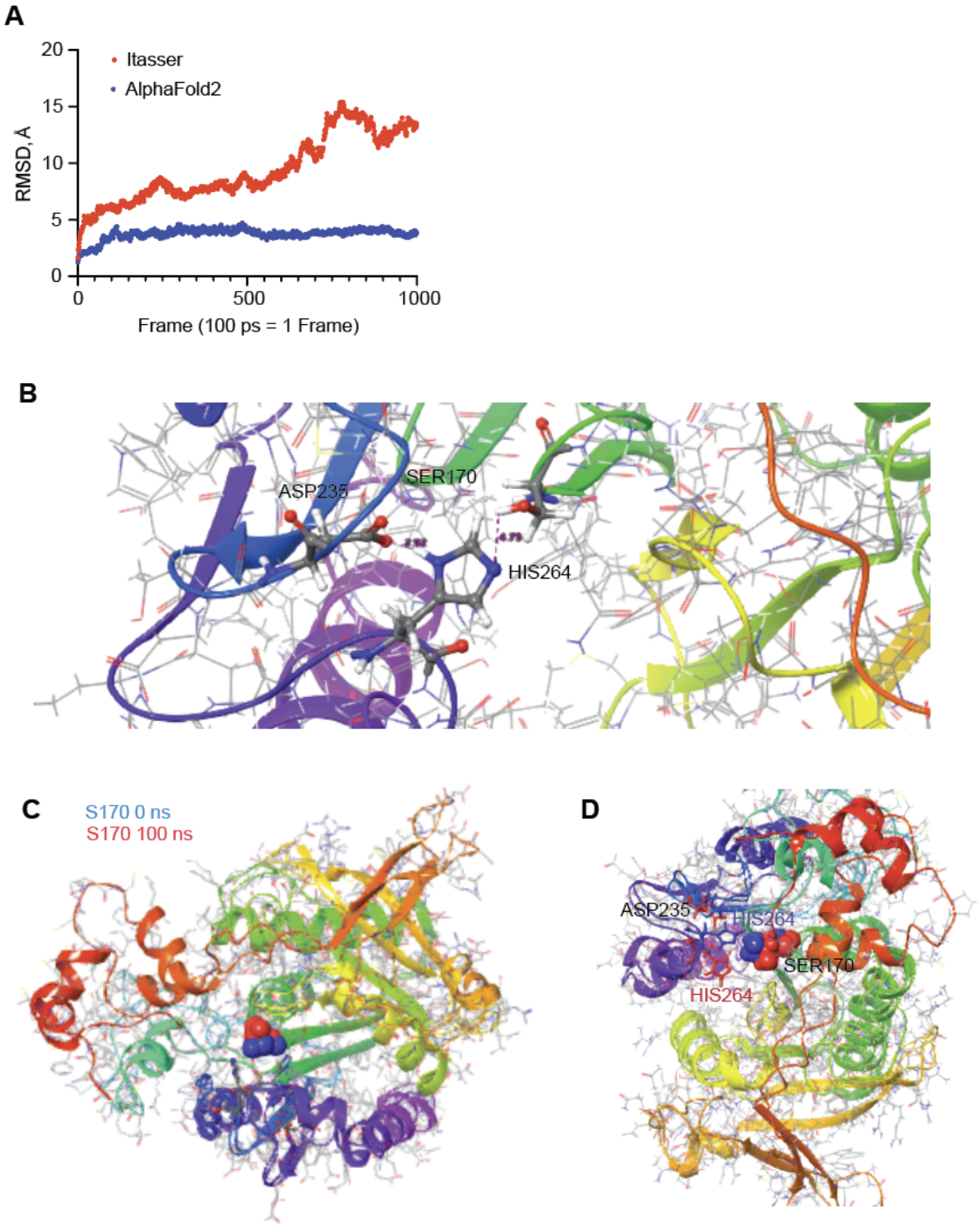
A
Itasser
AlphaFold2
RMSD, Å
20
15
10
5
0
0
500
1000
Frame (100 ps = 1 Frame)
B
ASP235
SER170
HIS264
C
S170 0 ns
S170 100 ns
D
ASP235
HIS264
SER170
HIS264

Supplementary Fig. 7. Modeling of ABHD17B and prediction of Ser170 as required for serine protease activity. (A) Root mean squared deviation (RMSD) of two simulations of ABHD17B generated through *de novo* protein folding either from I-Tasser server [57] (red) or AlphaFold2 (blue)[29]. (B) Representation of the potential catalytic triad of ABHD17B from AlphaFold2 minimized with OPLS3[80] as implemented in Maestro and equilibrated without production step from Namd2, indicating distances between Asp235 carboxylate oxygens and hydrogen of His264 as well as distance of deprotonated nitrogen of His264 and hydrogen of hydroxyl of Ser170. (C) Overlay of wildtype equilibrated ABHD17B at 0 and 100 ns with protein structure alignment in Maestro and Ser170 in space filling model with blue for 0 ns and red for 100 ns. (D) Aligned ABHD17B as in **Fig. 4** with catalytic triads indicated in red for 0 ns and blue for 100 ns in thicker line format indicating His264 as mobile due to positioning on flexible loop.

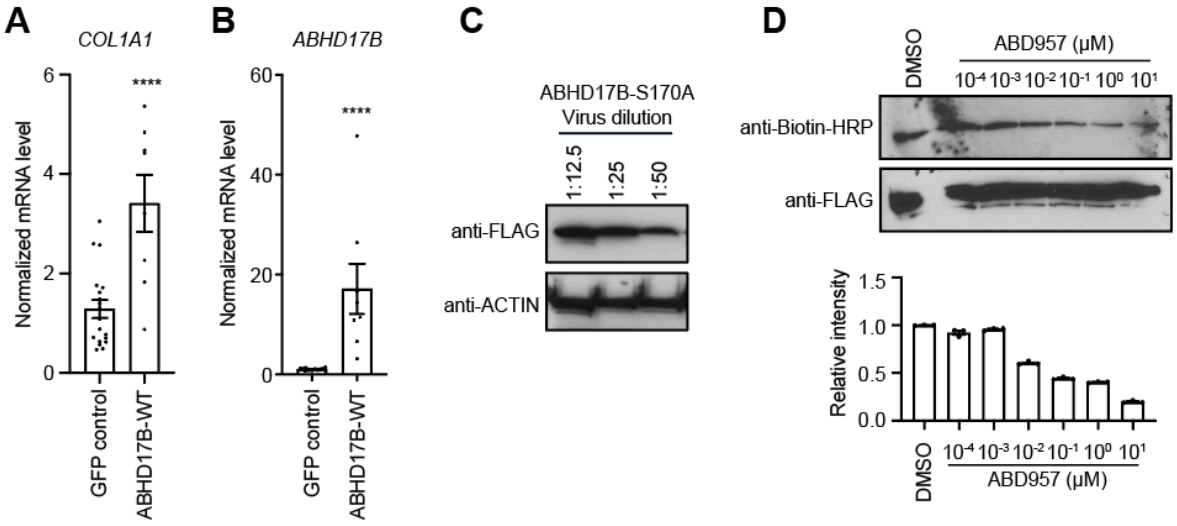
A
COL1A1
Normalized mRNA level
6
4
2
0
****
GFP control
ABHD17B-WT
B
ABHD17B
Normalized mRNA level
60
40
20
0
****
GFP control
ABHD17B-WT
C
ABHD17B-S170A
Virus dilution
1:12.5
1:25
1:50
anti-FLAG
anti-ACTIN
D
DMSO
ABD957 (μM)
10-4 10-3 10-2 10-1 100 101
anti-Biotin-HRP
anti-FLAG
Relative intensity
1.5
1.0
0.5
0.0
DMSO
10-4 10-3 10-2 10-1 100 101
ABD957 (μM)

Supplementary Fig. 8. Ectopic expression of ABHD17B and S170A ABHD17B and inhibition of depolmityolase activity with ABD957. (A) *COL1A1* mRNA expression was quantified by qRT-PCR in HSCs transduced with lentivirus expressing GFP-FLAG (GFP control) and wildtype ABHD17B-FLAG (ABDHD17B-WT). Error bars represent mean ± SEM (n=19 for GFP control, n=8 for ABHD17B-WT from four independent experiments). **** indicates p<0.0001 (t-test). (B) *ABHD17B* mRNA expression for the same samples shown in (A). Error bars represent mean ± SEM (n=19 for GFP control, n=8 for ABHD17B-WT from four independent experiments). **** indicates p<0.0001 (t-test). (C) Protein expression of S170A-ABHD17B-FLAG in HSCs as quantified by anti-FLAG antibody and anti-ACTIN antibody. Decreasing dilution of viral titers is indicated. Blot was performed to confirm ABDH17B-S170A-FLAG protein expression since the change in nucleotide sequence interfered with qRT-PCR amplification using the Taqman probe set (not shown). (D) Serine activity based probe assay (SABP) was performed to quantify the activity ABD957. HEK-293T cells were transfected with plasmids expressing wildtype (WT) ABHD17B-FLAG. Cells were lysed and then treated with a desthiobiotin-labeled serine based activity probe (SABP) on M2 anti-FLAG beads. Serine activity was quantified by streptavidin HRP, and protein levels bound to M2 beads were quantified by probing with anti-FLAG antibody. Concentrations of ABD957 are indicated. Band intensitied were quantified (bottom and normlaized to FLAG signal). Each band was quantified three times using Fiji. Error bars represent mean ± SEM. Results are representative of two independent experiments.

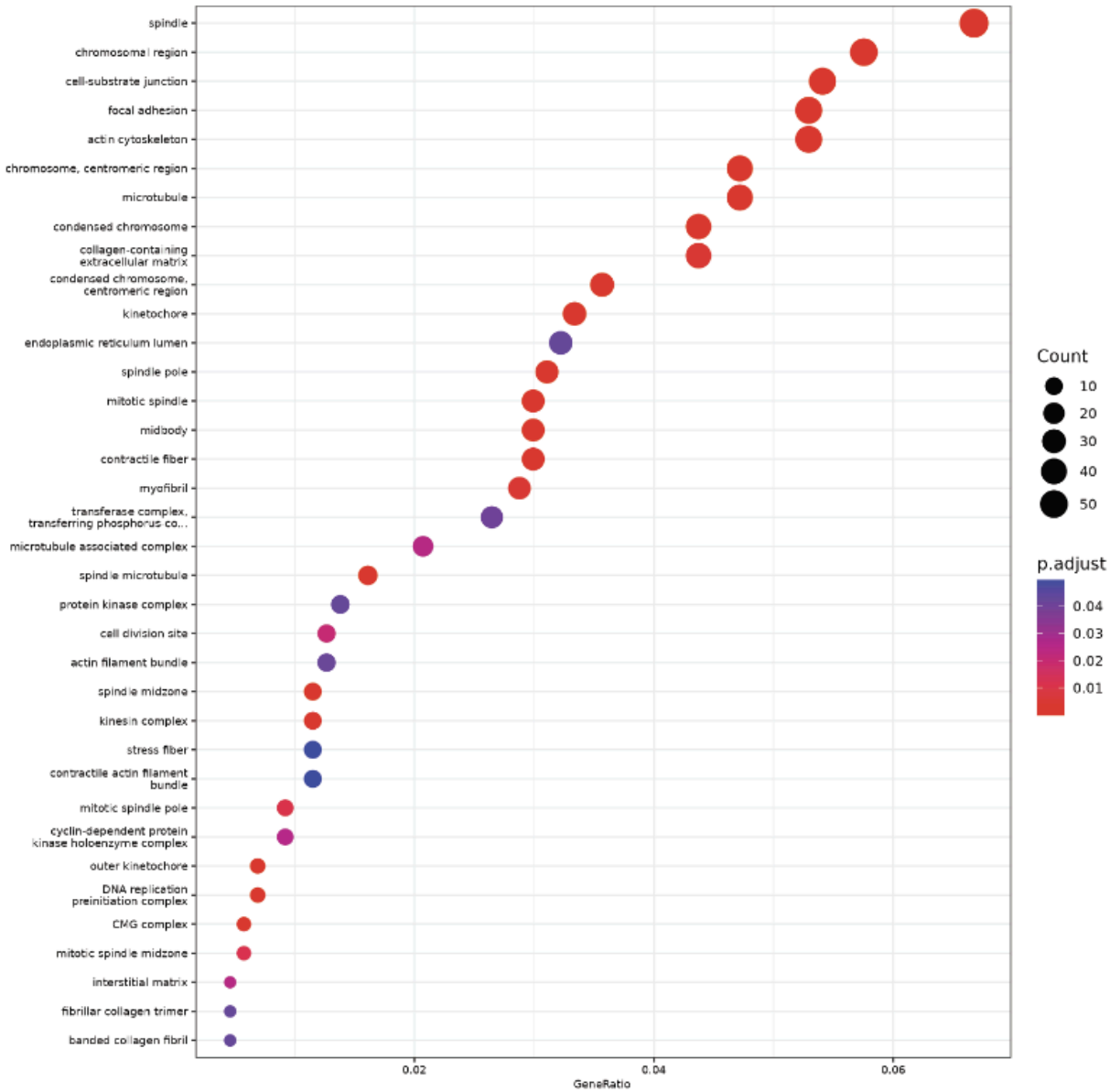
spindle
chromosomal region
cell-substrate junction
focal adhesion
actin cytoskeleton
chromosome, centromeric region
microtubule
condensed chromosome
collagen-containing extracellular matrix
condensed chromosome, centromeric region
kinetochore
endoplasmic reticulum lumen
spindle pole
mitotic spindle
midbody
contractile fiber
myofibril
transferase complex, transferring phosphorus co...
microtubule associated complex
spindle microtubule
protein kinase complex
cell division site
actin filament bundle
spindle midzone
kinesin complex
stress fiber
contractile actin filament bundle
mitotic spindle pole
cyclin-dependent protein kinase holoenzyme complex
outer kinetochore
DNA replication preinitiation complex
CMG complex
mitotic spindle midzone
interstitial matrix
fibrillar collagen trimer
banded collagen fibril
0.02
0.04
0.06
GeneRatio
Count
10
20
30
40
50
p.adjust
0.04
0.03
0.02
0.01

Supplementary Fig. 9. GO analysis for genes repressed with depletion of ABHD17B, **full map from Fig. 4A.** RNA sequencing and differential expression analysis were performed using nontargeting control (NTC) si5, and two siRNAs (siRNA#1 and #4) targeting *ABHD17B*. Dot plot displays the Gene Ontology (GO) terms most enriched as a result of ABHD17B depletion. The color of each dot represents the adjusted p-value, and the size of the dot represents gene count.

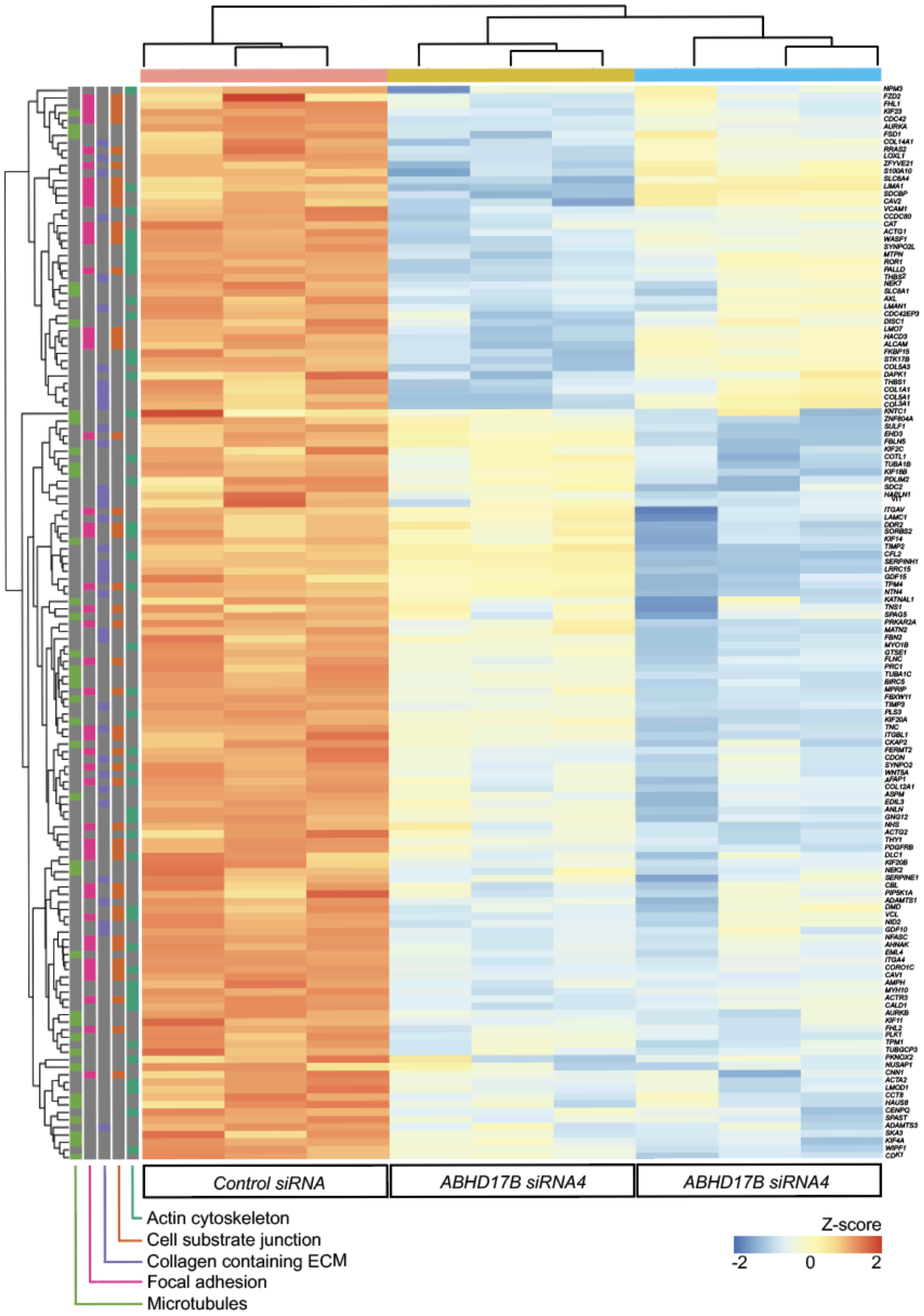
Control siRNA
ABHD17B siRNA4
ABHD17B siRNA4
Actin cytoskeleton
Cell substrate junction
Collagen containing ECM
Focal adhesion
Microtubules
Z-score
-2
0
2

Supplementary Fig. 10. Genes repressed with depletion of ABHD17B. Heatmap shows expression of the repressed gene set for indicated GO categories for HSCs transfected with NTC (C), siRNA #4 targeting *ABHD17B* and siRNA #1 targeting *ABHD17B.* Gene names are shown on the right. GO categories iindicated by color in the first five gray columns on the left. Expression is centered and scaled by row (gene). The Z-score scale for expression is shown in the lower right.

A

ABHD17B

ATGAATAATCTTTCATTTAGTGAGCTATGTTGCCTCTTCTGCTGTCCACCTTGTCCAGGGAA
GATTGCTTCAAAATTAGCGTTTTTGCCACCTGATCCAACTTACACACTGATGTGTGATGAAA
GCGGAAGCCGTTGGACTTTACATCTGTCTGAACGAGCAGACTGGCAGTATTCTTCTAGAGA
AAAAGATGCTATTGAGTGTTTCATGACTAGAACCAGTAAAGGCAACAGAATTGCTTGTATGT
TTGTACGTTGTTCACCCAATGCGAAATACACTTTACTCTTCTCACATGGAAATGCTGTTGAT
CTTGGTCAAATGAGCAGCTTTTACATAGGACTAGGATCACGGATTAATTGTAATATATTCTC
ATATGATTATTCTGGATATGGTGCCAGTTCCGGGAAACCCACAGAGAAGAACCTCTATGCA
GACATTGAAGCTGCTTGGCTTGCTCTTAGGACAAGATATGGCATTCGCCCTGAAAATGTGA
TTATATATGGCCAAAGTATAGGGACAGTACCGTCTGTGGATCTTGCTGCTCGATATGAGAG
TGCTGCTGTTATTCTTCATTCTCCTCTGACTTCGGGAATGCGAGTTGCCTTTCCaGAcACCA
AGAAGACCTACTGTTTTGATGCATTCCCAAACATTGACAAAATCTCTAAGATAACCTCTCCtG
TtcTAATAATTCATGGGACTGAAGATGAAGTCATTGACTTTTCACATGGCCTCGCATTGTTTG
AACGTTGCCAAAGACCTGTGGAGCCTCTCTGGGTTGAAGGAGCAGGTCACAATGATGTGG
AACTTTATGGACAGTATCTTGAAAGGTTGAAACAGTTTGTGTCACAGGAACTGGTAAATTTG

B

ABHD17B S170A

ATGAATAATCTTTCATTTAGTGAGCTATGTTGCCTCTTCTGCTGTCCACCTTGTCCAGGGAA
GATTGCTTCAAAATTAGCGTTTTTGCCACCTGATCCAACTTACACACTGATGTGTGATGAAA
GCGGAAGCCGTTGGACTTTACATCTGTCTGAACGAGCAGACTGGCAGTATTCTTCTAGAGA
AAAAGATGCTATTGAGTGTTTCATGACTAGAACCAGTAAAGGCAACAGAATTGCTTGTATGT
TTGTACGTTGTTCACCCAATGCGAAATACACTTTACTCTTCTCACATGGAAATGCTGTTGAT
CTTGGTCAAATGAGCAGCTTTTACATAGGACTAGGATCACGGATTAATTGTAATATATTCTC
ATATGATTATTCTGGATATGGTGCCAGTTCCGGGAAACCCACAGAGAAGAACCTCTATGCA
GACATTGAAGCTGCTTGGCTTGCTCTTAGGACAAGATATGGCATTCGCCCTGAAAATGTGA
TTATATATGGCCAAGCCATAGGGACAGTACCGTCTGTGGATCTTGCTGCTCGATATGAGAG
TGCTGCTGTTATTCTTCATTCTCCTCTGACTTCGGGAATGCGAGTTGCCTTTCCaGAcACCA
AGAAGACCTACTGTTTTGATGCATTCCCAAACATTGACAAAATCTCTAAGATAACCTCTCCtG
TtcTAATAATTCATGGGACTGAAGATGAAGTCATTGACTTTTCACATGGCCTCGCATTGTTTG
AACGTTGCCAAAGACCTGTGGAGCCTCTCTGGGTTGAAGGAGCAGGTCACAATGATGTGG
AACTTTATGGACAGTATCTTGAAAGGTTGAAACAGTTTGTGTCACAGGAACTGGTAAATTTG

Supplementary Fig. 11. Nucleotide sequence for *ABDH17B* and *S170A-ABHD17B*.

(A) The nucleotide sequence used to encode the wildtype (WT) amino acid sequence for ABHD17B is shown (top). The position of WT Ser 170 is indicated in red. Nucleotides in lower case blue text indicate changes from the endogenous nucleotide sequence that do not affect the amino acid sequence. The FLAG peptide was expressed at the C-terminus (not show). (B) The nucleotide sequence was mutated to change Ser 170 to Ala (indicated in red) for ABHD17B-S170A.